Cellular differentiation state modulates the mRNA export activity of SR proteins

Valentina Botti,[1]* François McNicoll,[2]* Michaela C. Steiner,[4]* Florian M. Richter,[3] Anfisa Solovyeva,[2] Marius Wegener,[2,5] Oliver D. Schwich,[2,5] Ina Poser,[4] Kathi Zarnack,[5] Ilka Wittig,[3] Karla M. Neugebauer,[1] and Michaela Müller-McNicoll[2]

[1]Department of Molecular Biophysics and Biochemistry, Yale University, New Haven, CT
[2]Cluster of Excellence Macromolecular Complexes, Institute of Cell Biology and Neuroscience and [3]Functional Proteomics Group, Institute for Biochemistry I, Goethe University Frankfurt, Frankfurt am Main, Germany
[4]Max Planck Institute of Molecular Cell Biology and Genetics, Dresden, Germany
[5]Buchmann Institute for Molecular Life Sciences, Frankfurt am Main, Germany

SR proteins function in nuclear pre-mRNA processing, mRNA export, and translation. To investigate their cellular dynamics, we developed a quantitative assay, which detects differences in nucleocytoplasmic shuttling among seven canonical SR protein family members. As expected, SRSF2 and SRSF5 shuttle poorly in HeLa cells but surprisingly display considerable shuttling in pluripotent murine P19 cells. Combining individual-resolution cross-linking and immunoprecipitation (iCLIP) and mass spectrometry, we show that elevated arginine methylation of SRSF5 and lower phosphorylation levels of cobound SRSF2 enhance shuttling of SRSF5 in P19 cells by modulating protein–protein and protein–RNA interactions. Moreover, SRSF5 is bound to pluripotency-specific transcripts such as *Lin28a* and *Pou5f1/Oct4* in the cytoplasm. SRSF5 depletion reduces and overexpression increases their cytoplasmic mRNA levels, suggesting that enhanced mRNA export by SRSF5 is required for the expression of pluripotency factors. Remarkably, neural differentiation of P19 cells leads to dramatically reduced SRSF5 shuttling. Our findings indicate that posttranslational modification of SR proteins underlies the regulation of their mRNA export activities and distinguishes pluripotent from differentiated cells.

Introduction

SR proteins are essential RNA-binding proteins (RBPs) with important functions in constitutive and alternative splicing (Änkö, 2014). The SR protein family comprises seven canonical members (SRSF1–SRSF7) that are structurally related but show divergent RNA-binding preferences in vivo (Müller-McNicoll et al., 2016). SR proteins contain one or two RNA recognition motifs (RRMs) at their N termini as well as a region of repeated serine-arginine dipeptides (RS domain) at their C termini. Most serine residues are extensively phosphorylated in the cytoplasm by SRPK1/2 and in the nucleus by Clk1/4 kinases (Aubol et al., 2013). Distinct phosphorylation states determine the different biological functions of SR proteins. Phosphorylation by SRPKs is essential for nuclear import and localization to nuclear speckles (Lai et al., 2001), hyperphosphorylation by Clks is crucial for recruitment to transcription sites and spliceosome assembly, and dephosphorylation by PP1/2A phosphatases during splicing is important for the release of the splicing machinery, recruitment of nuclear export factor 1 (NXF1), and export of mature mRNAs (Zhou and Fu, 2013).

SR proteins control cotranscriptional splicing (Sapra et al., 2009). Some family members perform additional post-splicing functions in nuclear and cytoplasmic processes such as 3′ end processing (Lou et al., 1998; Müller-McNicoll et al., 2016), mRNA export (Masuyama et al., 2004; Huang and Steitz, 2005), and translation (Michlewski et al., 2008; Maslon et al., 2014). In line with this, some SR proteins shuttle between the nucleus and the cytoplasm in HeLa cells (Cáceres et al., 1998; Cazalla et al., 2002; Sapra et al., 2009). The stimulatory effect of SRSF1 on translation is dependent on its ability to shuttle (Sanford et al., 2004; Michlewski et al., 2008), and importantly, inhibition of shuttling prevents its oncogenic potential (Shimoni-Sebag et al., 2013). It is currently unknown whether this applies to other SR protein family members, which have been implicated in several types of cancer (da Silva et al., 2015).

*V. Botti, F. McNicoll, and M.C. Steiner contributed equally to this paper.

Correspondence to Michaela Müller-McNicoll: mueller-mcnicoll@bio.uni-frankfurt.de; Karla M. Neugebauer: karla.neugebauer@yale.edu

Abbreviations used: BAC, bacterial artificial chromosome; CHX, cycloheximide; coIP, coimmunoprecipitation; esiRNA, endoribonuclease-prepared siRNA; FA, formic acid; FDR, false discovery rate; iCLIP, individual-nucleotide resolution cross-linking and immunoprecipitation; IP, immunopurification; LC, liquid chromatography; LFQ, label-free quantification; MEF, mouse embryonic fibroblast; mRNP, messenger RNP; MS, mass spectrometry; NRS, nuclear retention sequence; OE, overexpression; PTM, posttranslational modification; RBP, RNA-binding protein; RRM, RNA recognition motif; TRN, transportin.

Supplemental material can be found at:
http://doi.org/10.1083/jcb.201610051

The Rockefeller University Press
J. Cell Biol. Vol. 216 No. 7 1993–2009
https://doi.org/10.1083/jcb.201610051

Absence of shuttling was reported for SRSF2 and SRSF5 in HeLa cells (Cáceres et al., 1998; Cazalla et al., 2002; Sapra et al., 2009) and mouse embryonic fibroblasts (MEFs; Lin et al., 2005). The inability of SRSF2 to shuttle is caused by a hydrophobic nuclear retention sequence (NRS) located within its RS domain, conferring resistance to phosphatases (Cazalla et al., 2002). Because SRSF2 remains phosphorylated after splicing, it is unable to recruit NXF1 and must be removed from messenger RNPs (mRNPs) before export (Lin et al., 2005). In contrast, SRSF5 lacks a recognizable NRS, and its shuttling disability is not understood. It is also unknown whether SR protein shuttling differs between cellular conditions.

In this study, we have developed a quantitative shuttling assay and measured the nucleocytoplasmic shuttling of SR proteins in different cell types. To our surprise, SRSF2 and SRSF5 shuttle considerably in pluripotent but not in differentiated cells. We provide evidence that the inability of SRSF5 to shuttle in differentiated cells is caused by cobinding of phosphatase-resistant SRSF2 and impeded NXF1 recruitment. Conversely, in pluripotent cells, higher arginine methylation levels of SRSF5, enhanced binding to mature mRNAs, and partial dephosphorylation of SRSF2 contribute to stable NXF1 binding and shuttling of both SRSF2 and SRSF5. Adapting individual-nucleotide resolution cross-linking and immunoprecipitation (iCLIP) to polysome-associated transcripts (PiCLIP), we show that SRSF5 binds to pluripotency-specific transcripts undergoing translation. Moreover, SRSF5 knockdown affects their nucleocytoplasmic distribution, suggesting additional functions for SRSF5 in pluripotent cells.

Results

A quantitative assay reveals differences in shuttling capacities of SR protein family members

Shuttling of RBPs between the nucleus and cytoplasm indicates their potential to carry cargo between compartments and is usually assessed qualitatively using heterokaryon assays. The original assay involves the fusion of human and mouse cells to produce interspecies heterokaryons, in which the donor cell carries a fluorescently tagged protein. Fused cells are identified by phase-contrast microscopy, donor and recipient nuclei are identified by distinct chromatin features (Borer et al., 1989), and heterokaryons are scored for fluorescence in recipient nuclei. This assay is laborious, subjective, and typically yields very few examinable heterokaryons. To increase the reliability and efficiency of this assay and to allow quantitative measurements we used recipient HeLa cells stably expressing the membrane marker CAAX-mCherry (Wright and Philips, 2006).

SR proteins are not detectable in the cytoplasm at steady state (Fig. 1 A). To compare their shuttling abilities, we used clonal donor bacterial artificial chromosome (BAC) cell lines expressing seven canonical SR proteins (SRSF1–SRSF7) with a GFP tag from genomic loci in pluripotent mouse P19 cells (Fig. S1 A; Müller-McNicoll et al., 2016). GFP-tagged SR proteins are expressed at endogenous levels, recapitulate mRNA binding patterns of their endogenous counterparts, are functional in splicing (Änkö et al., 2010, 2012), are phosphorylated in vivo, and localize to nuclear speckles (Fig. S1, B and C).

Within a heterokaryon, shuttling SR proteins can be reimported either into donor P19 or into recipient HeLa nuclei, which can be quantified as newly emerging GFP fluorescence (Fig. 1 A). To readily identify true heterokaryons (nuclei from two different species in a shared cytoplasm), we screened for fusion events showing GFP expression (P19) surrounded by a plasma membrane labeled with CAAX-mCherry (HeLa; Fig. 1 A). P19 and HeLa nuclei were confirmed by their distinct Hoechst staining patterns (Fig. 1 A).

Stable cell lines expressing GFP-tagged NXF1 and the spliceosomal component PRPF8-GFP were used as positive and negative controls (Fig. 1 B). Inspection of heterokaryons revealed that PRPF8-GFP was absent from receiving HeLa cell nuclei, whereas NXF1-GFP fluorescence was evenly distributed between both nuclei (Fig. 1 B). Interestingly, all seven SR proteins showed GFP fluorescence in receiving HeLa nuclei, but with visible differences in signal intensity (Figs. 1 C and S1 D). To quantify the shuttling capacities, z stacks of 30 heterokaryons per fusion were acquired, and percent GFP fluorescence in receiving HeLa nuclei was calculated as described in the Quantification of shuttling capacities section of Materials and methods. Equal fluorescence in donor and recipient nuclei was attained by NXF1, showing that 3 h after fusion was sufficient to reach shuttling equilibrium (Fig. 1 D). To exclude nonspecific effects, two different protein synthesis inhibitors, puromycin and cycloheximide (CHX), were used (Fig. S1 E). Quantification confirmed that all SR proteins undergo nucleocytoplasmic shuttling, albeit to different extents. Pairwise comparisons distinguished three shuttling groups: SRSF1, SRSF3, and SRSF7 (“high shuttlers”), SRSF2 and SRSF5 (“intermediate shuttlers”), and SRSF4 and SRSF6 (“low shuttlers”), which showed weak yet significant shuttling compared with the negative control PRPF8 (Table S1). This analysis indicates that all SR protein family members undergo nucleocytoplasmic shuttling in pluripotent P19 cells, but their mRNA export or cytoplasmic functions may vary.

Shuttling correlates with phosphorylation sites, NXF1 interaction, and presence in polysomal fractions

We next investigated which factors influence nucleocytoplasmic shuttling. Shuttling capacities correlated inversely with RS domain length and the number of serine residues therein (Figs. 2 A and S2 A). Moreover, shuttling was proportional to the extent of NXF1 interaction (Figs. 2 B and S2 B; Müller-McNicoll et al., 2016). Only hypophosphorylated SR proteins recruit NXF1, and SR proteins with long RS domains might be less efficiently dephosphorylated during splicing; consequently, they might bind less NXF1 (Huang and Steitz, 2005). Shuttling also correlated inversely with the number of tyrosine and serine residues within the NXF1 interaction region (Fig. S2 C), whose phosphorylation might affect NXF1 binding (Hargous et al., 2006; Tintaru et al., 2007).

We then compared SR protein abundance in cytoplasmic fractions containing translating polysomes. A subset of SRSF1-, SRSF3-, and SRSF7-GFP cosedimented with 80S ribosomes and light polysomes as previously reported (Fig. 2 C; Sanford et al., 2004; Swartz et al., 2007). Interestingly, SRSF5 also cosedimented with light polysomes, confirming that SRSF5 is partly cytoplasmic in P19 cells, whereas SRSF2 and the low shuttlers SRSF4 and SRSF6 were excluded from these fractions (Fig. 2 C). A GFP-NLS control did not cosediment with 80S or polysomal fractions (Fig. S2 D). We conclude that the shuttling capacities of individual SR proteins correlate with the number of

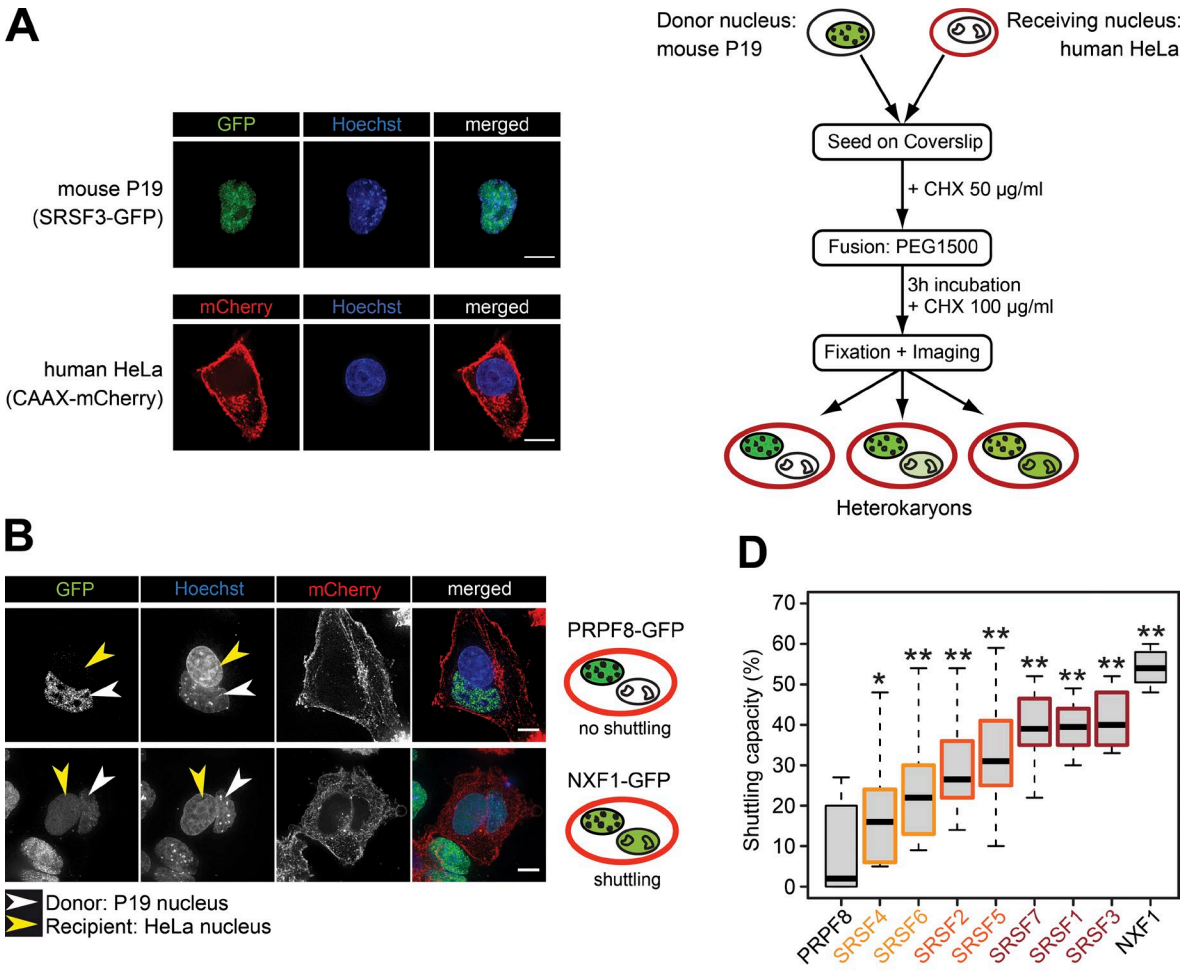

potential phosphorylation sites, NXF1 interaction, and presence in polysomal fractions, suggesting additional cytoplasmic functions for highly shuttling SR proteins in pluripotent P19 cells.

SRSF5 shows cell type–specific differences in shuttling and NXF1 interaction

Intermediate shuttling of SRSF2 and SRSF5 in P19 cells was surprising, as previous studies reported a complete absence of shuttling in HeLa cells and MEFs using nonquantitative heterokaryon assays (Cáceres et al., 1998; Lin et al., 2005; Sapra et al., 2009). To exclude that the GFP-tag masks the NRS of SRSF2, we performed inverse shuttling assays in which HeLa cells expressing GFP-tagged SRSF2, SRSF3, SRSF5, and SRSF7 (Sapra et al., 2009) were fused with WT P19 cells (Fig. 3, A and B). Quantification revealed that SRSF3 and SRSF7 shuttle in both cell types; however, SRSF2 and SRSF5 did not shuttle when HeLa cells were donors, indicating that the NRS was functional. To exclude the possibility that CAAX-mCherry expression affects HeLa nuclei, forward shuttling assays with HeLa WT cells were performed wherein fused membranes were stained with CellMask, yielding similar results (unpublished data). To confirm shuttling of SRSF2 and SRSF5 in P19 cells, nuclear import of SR proteins was blocked for 3 h using actinomycin D (ActD) in the presence of CHX, which lead to a clear accumulation of SRSF2 and SRSF5 in the cytoplasm (Fig. S2 E; Cáceres et al., 1998).

In agreement with their inability to shuttle in HeLa cells, SRSF2- and SRSF5-GFP did not cosediment with polysomes (Fig. 3 C) and were absent from NXF1-containing mRNPs (Figs. 3 D and S2 F). In contrast, a subset of SRSF5-GFP interacted with NXF1 independently of RNA in P19 cells (Figs. 3 D and S2 F) and was detectable in light polysomal fractions (Figs. 2 C and 3 C). In summary, we discovered that SRSF2 and SRSF5 are exported to the cytoplasm in pluripotent P19 cells, suggesting cell type–specific differences in SR protein shuttling.

Arginine methylation in the SRSF5–NXF1 interaction region varies among cell types and affects shuttling

Shuttling comprises active nuclear export of SR proteins via NXF1 and reimport by the importin transportin (TRN; TRN-SR), which requires rephosphorylation of SR proteins by SRPK1/2 (Huang and Steitz, 2005). The capacity of SRSF5 to shuttle in P19 cells correlated with an enhanced NXF1 interaction (Fig. 3 D) as well as a 1.8-fold higher NXF1 and TRN-SR expression compared with HeLa cells (Fig. S3 A). Cross-species transfection experiments excluded differences in the primary protein sequence to account for the shuttling differences (not depicted).

The correlation with potential phosphorylation sites (Fig. 2) prompted us to test whether SRSF5 is differently phosphorylated in HeLa and P19 cells. Western blots using the mAb104 antibody, which recognizes phosphorylated RS domains of all canonical SR proteins (Zahler et al., 1993), suggested higher phosphorylation levels or abundance of SRSF5 in P19 cells (Fig. 4 A). To dissect this, we assayed the migration of SRSF5-GFP in Phos-tag gels using anti-GFP antibodies. SRSF5-GFP was indeed more abundant in P19 cells; however, both proteins showed a similar migration pattern without size shift, strongly suggesting that SRSF5 is similarly phosphorylated in P19 and HeLa cells (Fig. 4 B).

We failed to validate similar RS domain phosphorylation of SRSF5-GFP by quantitative mass spectrometry (MS; also see the Sample preparation and MS section of Materials and methods) because of the high charge and repetitive nature of the RS domains. However, quantifying other posttranslational modifications (PTMs) using spectral counting revealed more robust arginine methylations within the putative NXF1-interacting domain of SRSF5-GFP in P19 cells, with dimethyl residues especially on R_{88}, R_{92}, and R_{93}, whereas monomethylations dominated in HeLa cells (Fig. 4 C). Stringent immunopurifications (IPs) probed with methylation-specific antibodies confirmed lower arginine dimethylation levels of SRSF5-GFP in HeLa (not depicted); however, methylation at other residues was similar in both cells, ruling out general differences in methylation activities (Fig. S3 B).

In vitro studies showed that arginine residues corresponding to R_{92} and R_{93} are essential for NXF1 binding in SRSF1 and SRSF7 (Hargous et al., 2006; Tintaru et al., 2007). We mutated R_{92} and R_{93} in SRSF5 and the corresponding R_{105} and R_{106} in SRSF3 to alanines on BACs (Fig. 4 D). Mutant proteins showed similar expression to WT proteins in stable clonal BAC cell lines (Fig. S3 C). Strikingly, interaction of $SRSF3_{R105,106A}$ and $SRSF5_{R92,93A}$ with NXF1 was significantly decreased (Figs. 4 E and S3 D), indicating that these residues are also important for NXF1 binding to SRSF3 and SRSF5 in vivo. Importantly, $SRSF5_{R92,93A}$ also showed significantly reduced shuttling compared with WT SRSF5 (Figs. 4 F and S3 E). Altogether, our data show that the extent of NXF1 binding determines the shuttling capacities of SR proteins and suggest that robust methylation of arginine residues flanking the NXF1 interaction region enhances NXF1 binding and shuttling of SRSF5 in pluripotent P19 cells.

SRSF5 shows differences in target binding and association with mature mRNPs

Further inspection of quantified PTMs revealed that aromatic residues at the end of RRM2 were more oxidized in HeLa cells (Fig. S3 B), suggesting differential protection from oxidization, possibly by bound RNA. Indeed, quantification of SRSF5 peptides from RRM2 revealed between 3- and 41-fold more cross-linking to RNA in P19 cells compared with HeLa cells (Figs. S3 B and S4 A; also see the MS data analysis section of Materials and methods). Differential contribution of both RRMs to RNA binding may result in the recognition of different RNA targets in P19 and HeLa cells. To test this, we performed iCLIP of SRSF5- and SRSF2-GFP expressed in HeLa cells (H) and compared the results to data obtained with P19 cells (Fig. S4, B and C; Müller-McNicoll et al., 2016). Replicates were

Figure 1. **A quantitative assay reveals differences in shuttling capacities of SR protein family members.** (A, left) Nuclear SRSF3-GFP and bright heterochromatic dots upon Hoechst staining in P19 cells (top) and HeLa cells expressing CAAX-mCherry (bottom). (Right) Workflow of quantitative shuttling assay. (B) Representative fusion events for PRPF8-GFP and NXF1-GFP shown as projections of three z stacks. (C) Representative fusion events for seven SR proteins ordered by their shuttling capacities. Colors indicate shuttling groups: low (light orange), medium (dark orange), and high shuttlers (red; also see Table S1). Images contain unfused HeLa cells (asterisks) used for background subtraction. Bars, 10 µm. (D) Percent GFP fluorescence in receiving nuclei after background subtraction as a measure of shuttling capacities (n = 30 heterokaryons per SR protein). Coloring is as in C. *, $P < 0.05$; **, $P < 0.001$ (Student's t test). Box plot shows median, 25th and 75th percentiles, and outermost data points.

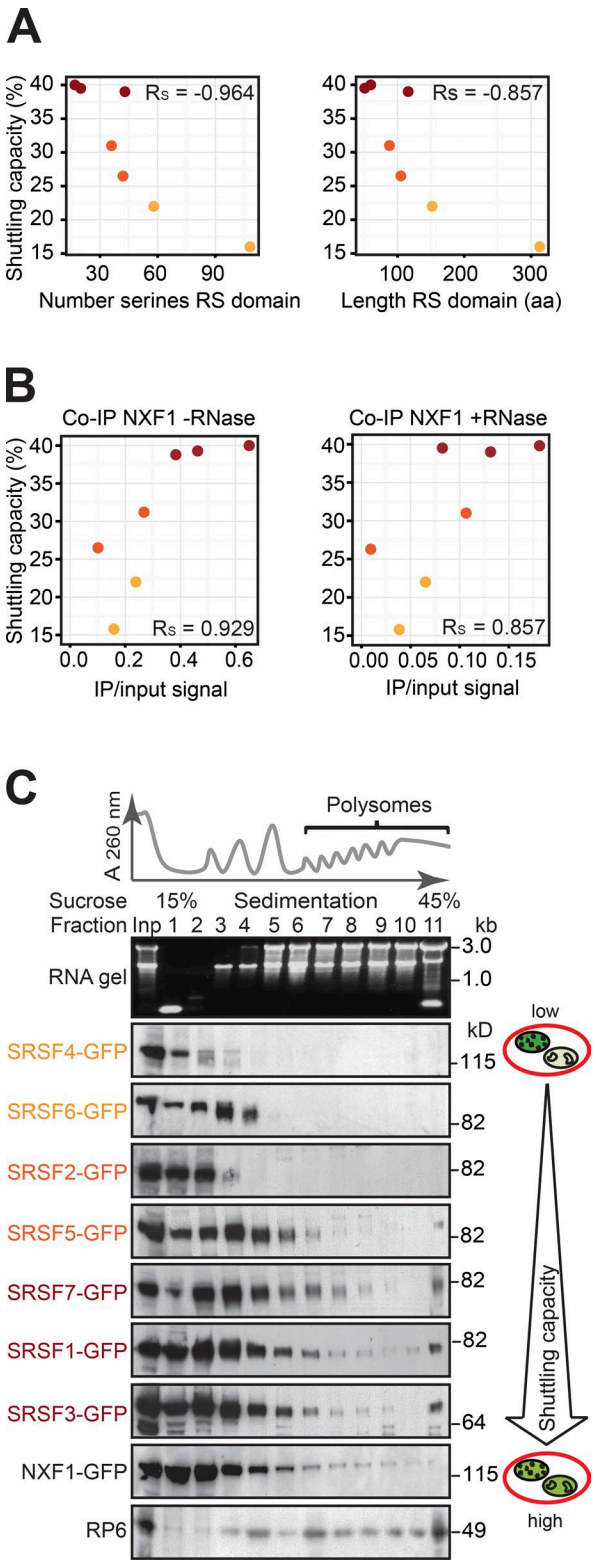

Figure 2. **Shuttling correlates with phosphorylation sites, NXF1 interaction, and presence in polysomal fractions.** (A) Comparison of median shuttling capacities quantified from 30 heterokaryons to the number of serines and RS domain length. Spearman's rank order correlation coefficients (Rs) are shown. Coloring is as in Fig. 1 (C and D). (B) Comparison of median shuttling capacities to NXF1 interaction, quantified from six forward coIP experiments using GFP-tagged SR proteins and endogenous NXF1 with (right) and without (left) RNase A treatment (Müller-McNicoll et al., 2016). (C) Western blot analysis of GFP-tagged SR proteins in P19 cell extracts fractionated across 15–45% sucrose gradients. An RNA gel confirms ribosome integrity. Fractions 5–11 contain translating ribosomes, and fractions 1–4 are ribosome-free. The ribosomal protein RP6 served as control. A 260, absorption at 260 nm; Inp, input.

reproducible (Table S2), and pooled reads yielded 1,783,089 and 1,017,813 unique cross-link events for SRSF2(H) and SRSF5(H), respectively, corresponding to 316,296 and 131,453 significant binding sites in 6,554 and 2,795 protein-coding target mRNAs (Table S3). The correlation between binding events and target expression (read count) was low (Fig. 5 A). Although SRSF2 targets were largely similar in both cell types (70/61% overlap), SRSF5 targets had very little overlap (37/29%), despite comparable numbers of cross-link events in P19 cells (Fig. 5 B). Unique P19 targets were enriched in categories such as cell morphogenesis, neural differentiation, and development, and ∼30% were not expressed or were very weakly expressed in HeLa cells (Fig. 5 C), suggesting specific roles for SRSF5 in pluripotent cells. In contrast, unique HeLa targets were enriched in categories related to DNA repair and replication (Figs. 5 C and S4 D).

Structural studies indicated that RRM1 recognizes preferentially pyrimidine-rich motifs, whereas RRM2 recognizes GGA (Cléry et al., 2008). The HeLa SRSF5-GFP in vivo binding motif consisted of U(U)C followed by GG or GA, suggesting that both RRMs contribute to RNA binding (Fig. 5 D). Interestingly, P19 SRSF5-GFP iCLIP yielded two distinct in vivo binding motifs, which resembled the HeLa motif in nucleotide identity but in a scrambled order (Fig. 5 D). Comparison of cross-link patterns revealed that SRSF2 and SRSF5 cross-link more to intronic and noncoding regions in HeLa cells compared with a preferential association with exonic and coding regions in P19 cells (Figs. 5 E and S4 E, gray arrows). Moreover, both proteins cross-link significantly less to spliced junctions in HeLa cells (Fig. 5 F), suggesting that they are removed from mature mRNAs before export as proposed previously (Lin et al., 2005). In contrast, SRSF2 and SRSF5 cross-link to a considerable fraction of spliced mRNAs in pluripotent P19 cells, suggesting that both proteins remain bound to mRNAs after splicing. Altogether, our data strongly suggest that both RRMs of SRSF5 bind to RNA, but their different contribution as well as differences in mRNA expression in both cell types result in distinct binding motifs, patterns, and target RNAs.

Partial dephosphorylation of SRSF2 promotes shuttling of SRSF5 in P19 cells

Although both SRSF2 and SRSF5 clearly shuttled in P19 cells, SRSF2 was not detectable in polysomal fractions in either cell type (Figs. 2 C and 3 C). In P19 cells, a subset of SRSF2 was present in NXF1-containing mRNPs, but this interaction was mediated via RNA (Fig. 3 D). To test whether SRSF2-GFP shuttling requires NXF1, we performed shuttling assays with P19 cells expressing SRSF2-GFP after NXF1 knockdown (Figs. 6 A and S5 A). SRSF3-GFP was used as a control for NXF1-dependent shuttling. Only modest reductions in NXF1 levels (by 25–33%) could be achieved (Fig. S5 B), yet a significant reduction in shuttling of SRSF2-GFP was observable (Fig. 6 A), suggesting that shuttling of SRSF2 depends on NXF1.

Previous studies using HeLa and MEFs suggest that SRSF2 is unable to recruit NXF1 because it is resistant to dephosphorylation and must be removed from the mRNP before

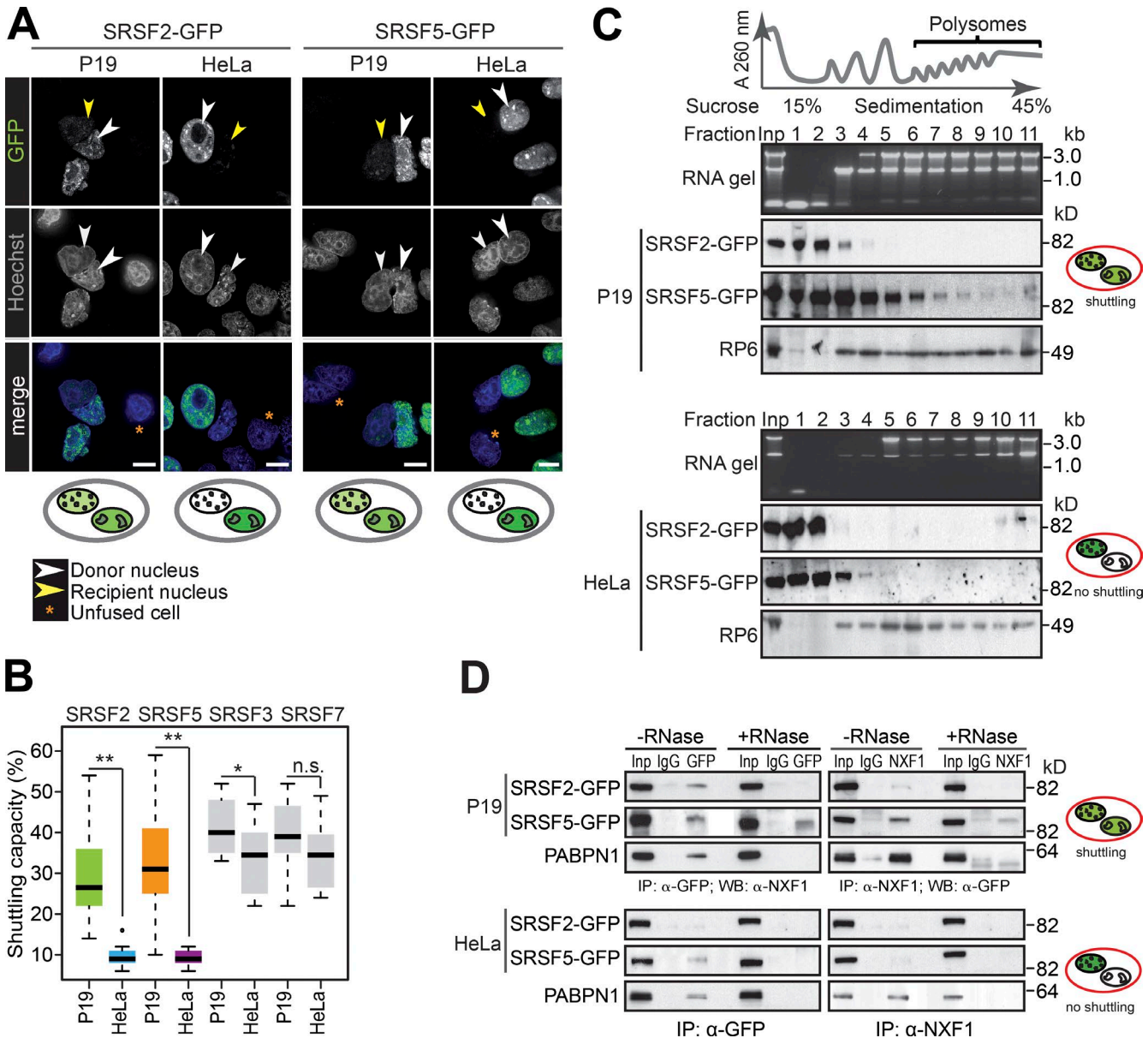

Figure 3. **SRSF5 shows cell type–specific differences in shuttling and NXF1 interaction.** (A) Representative fusion events for SRSF2-GFP and SRSF5-GFP in forward (P19 donor) and reverse (HeLa donor) shuttling assays. Bars, 10 µm. (B) Quantification of 25 heterokaryons per condition. *, $P < 0.05$; **, $P < 0.001$ (two-sided Wilcoxon rank-sum test). (C) Western blotting analysis for SRSF2-GFP and SRSF5-GFP in polysomal fractions. A 260, absorption at 260 nm. (D) Representative forward and reverse coIP experiments of SRSF2-GFP and SRSF5-GFP with NXF1. PABPN1 served as control for RNA-dependent interaction. Inp, input. Note that SRSF5 was run in inverse order.

export (Cazalla et al., 2002; Lin et al., 2005). Our data, however, indicate that a significant subset of SRSF2 binds mature spliced mRNAs (Fig. 5, E and F) in P19 cells. To assess the phosphorylation state of mRNA-bound SRSF2, we performed oligo(dT) capture assays followed by Phos-tag gel analysis from UV–cross-linked P19 cells. Similarly to SRSF5-GFP, the bulk of SRSF2-GFP cross-linked to mature poly(A)$^+$ RNAs was hypophosphorylated (Fig. 6 B). Phos-tag gel analysis of sucrose gradient fractions confirmed that hypophosphorylated SRSF2-GFP remained excluded from polysomes, in contrast to SRSF5-GFP, which associated with polysomes in its hypophosphorylated state (Fig. 6 C, red asterisks). This suggests that SRSF2 was removed from mRNAs shortly after export. We confirmed that SRSF2-GFP was more phosphatase-sensitive and readily dephosphorylated by calf intestinal phosphatase in P19 cells (Fig. 6 D) and that its steady-state phosphorylation level was lower than in HeLa cells (Figs. 6 E and S5 C). In contrast, SRSF5-GFP showed no differences in phosphorylation level and phosphatase resistance between these two cell lines (Figs. 4 C and 6 D).

SRSF2 and SRSF5 have similar shuttling capacities (Fig. 1 D) and tend to bind the same mRNAs in the same exons (90% shared targets and cobound exons; Fig. S5, D, F, and G; Müller-McNicoll et al., 2016). We thus hypothesized that SRSF2 might shuttle passively via SRSF5-containing mRNPs. Both proteins bound at ∼50 nt from splice sites but without any preference for a position or a splice site (Fig. S5 G). To test whether SRSF2 and SRSF5 bind side-by-side on the same

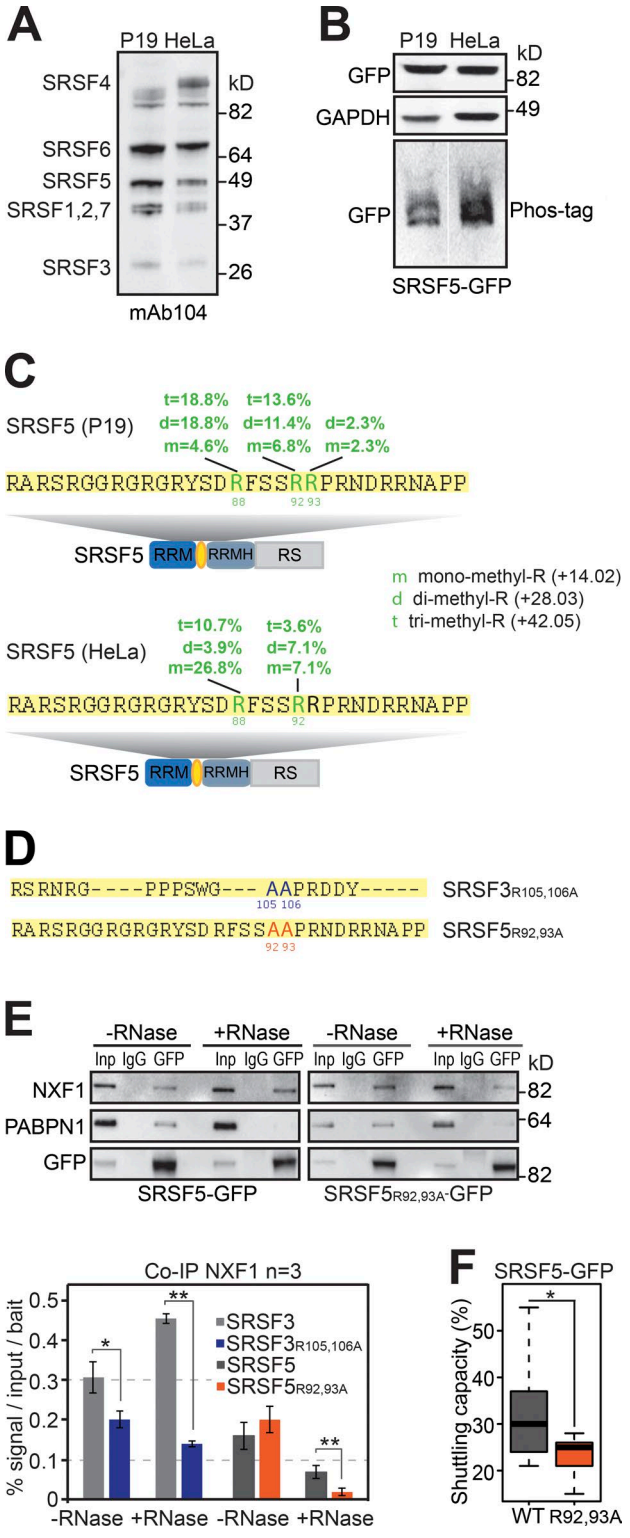

Figure 4. **Arginine methylation in the NXF1 interaction region varies between cell types and affects shuttling.** (A) Phosphorylated SR proteins were detected by Western blotting using mAb104. (B) SRSF5-GFP was detected with anti-GFP antibodies on normal (top) and Phos-tag SDS-PAGE gels (bottom). GAPDH was used as a loading control. Note that the Phos-tag gel was run with an empty lane between samples, which was removed in the figure. (C) SRSF5-GFP was analyzed by tandem MS to obtain semiquantitative information on PTMs using spectral counting. Modified arginines within the putative NXF1 interaction region (yellow) are labeled in green with the percentage of modification compared with all detected peptides. Changes of mass are indicated in parentheses. Trimethylation has to be interpreted as a combination of di- and monomethylation on neighboring residues. Summary of eight (P19) and six (HeLa) replicates. (D) Schematic of serine-to-alanine substitutions in SRSF3 and SRSF5. (E) CoIPs of WT and mutated SRSF3-GFP or SRSF5-GFP with NXF1. (Top) Representative experiment for SRSF5-GFP and $SRSF5_{R92,93A}$-GFP. Inp, input. (Bottom) Quantification of three independent experiments normalized to baits and inputs. *, $P < 0.05$; **, $P < 0.001$ (Student's *t* test). Error bars indicate SEM. (F) Quantification of 15 heterokaryons per protein variant. *, $P < 0.01$ (two-sided Wilcoxon rank-sum test).

RNAs or compete for binding sites, we developed a proximity-interactome capture protocol involving UV cross-linking, differential RNase digestion, and MS, which allowed us to identify all proteins that bound in very close proximity to a protein of interest on the same RNAs in vivo (Fig. 6 F, see the Sample preparation and MS section of Materials and methods). Label-free quantification (LFQ) was used to identify significantly enriched proteins compared with noncross-linked (UV^-) samples. In agreement with the coimmunoprecipitation (coIP) data, SRSF5 interacts exclusively in P19 cells with NXF1, and both proteins bind in close proximity on the same RNA as proposed recently (Müller-McNicoll et al., 2016). In contrast, NXF1 was absent in the HeLa interactomes (Fig. 6 G; Fig. S5 H; and Tables S4, S5, S6, and S7). More importantly, SRSF2 was the most enriched SR protein in UV^+ SRSF5-GFP proximity interactomes in P19 cells, whereas their interaction was more RNA-independent in HeLa cells (Figs. 6 G and S5 H). The preferential and RNase-sensitive association of SRSF2 and SRSF5 was confirmed by reverse coIP experiments (Fig. 6 H).

Altogether, our data suggest that in pluripotent P19 cells, a subset of SRSF2 is dephosphorylated after splicing and remains bound to mature mRNAs. In contrast, SRSF2 is more phosphatase-resistant in HeLa cells and remains hyperphosphorylated after splicing. SRSF2 and SRSF5 bind frequently in close proximity on the same mRNAs in both cell types, but only in P19 cells, SRSF5 recruits NXF1 to the mRNP, potentially enabling SRSF2 to shuttle to the cytoplasm as a "passive passenger." Conversely, impaired recruitment of NXF1 by SRSF5 in HeLa cells may cause both proteins to remain nuclear.

SRSF5 binds to pluripotency-specific transcripts in polysomal fractions and affects their nucleocytoplasmic distribution

Enhanced binding of SRSF5 to mature mRNAs and its presence in polysomal fractions in P19 cells suggest that it may accompany bound mRNAs to ribosomes. To test this, we developed iCLIP from polysomal fractions (PiCLIP). SRSF3-GFP was used as a positive control, as it was shown to associate with polysomes (Kim et al., 2014). Polysome profiles (UV^+) were highly reproducible and indistinguishable from those obtained with noncross-linked samples (Figs. 2 C, 3 C, and 7 A). PiCLIP libraries were prepared from pooled monosomal (5 and 6) or polysomal fractions (7–10; Fig. 7 B). Biological replicates correlated well and were pooled to calculate significant cross-link events. Both proteins cross-linked to RNAs in cytoplasmic fractions, and the small overlap suggests target specificity (Fig. S5 I). For SRSF5, cross-linking to 5′ UTRs and open reading frames was strongly reduced compared with total RNA iCLIP (Müller-McNicoll et al., 2016), whereas cross-link densities within 3′ UTRs remained similar (Fig. 7 D). This suggests that SRSF5 is removed from 5′ UTRs/coding regions by scanning/translating ribosomes but remains bound within 3′ UTRs.

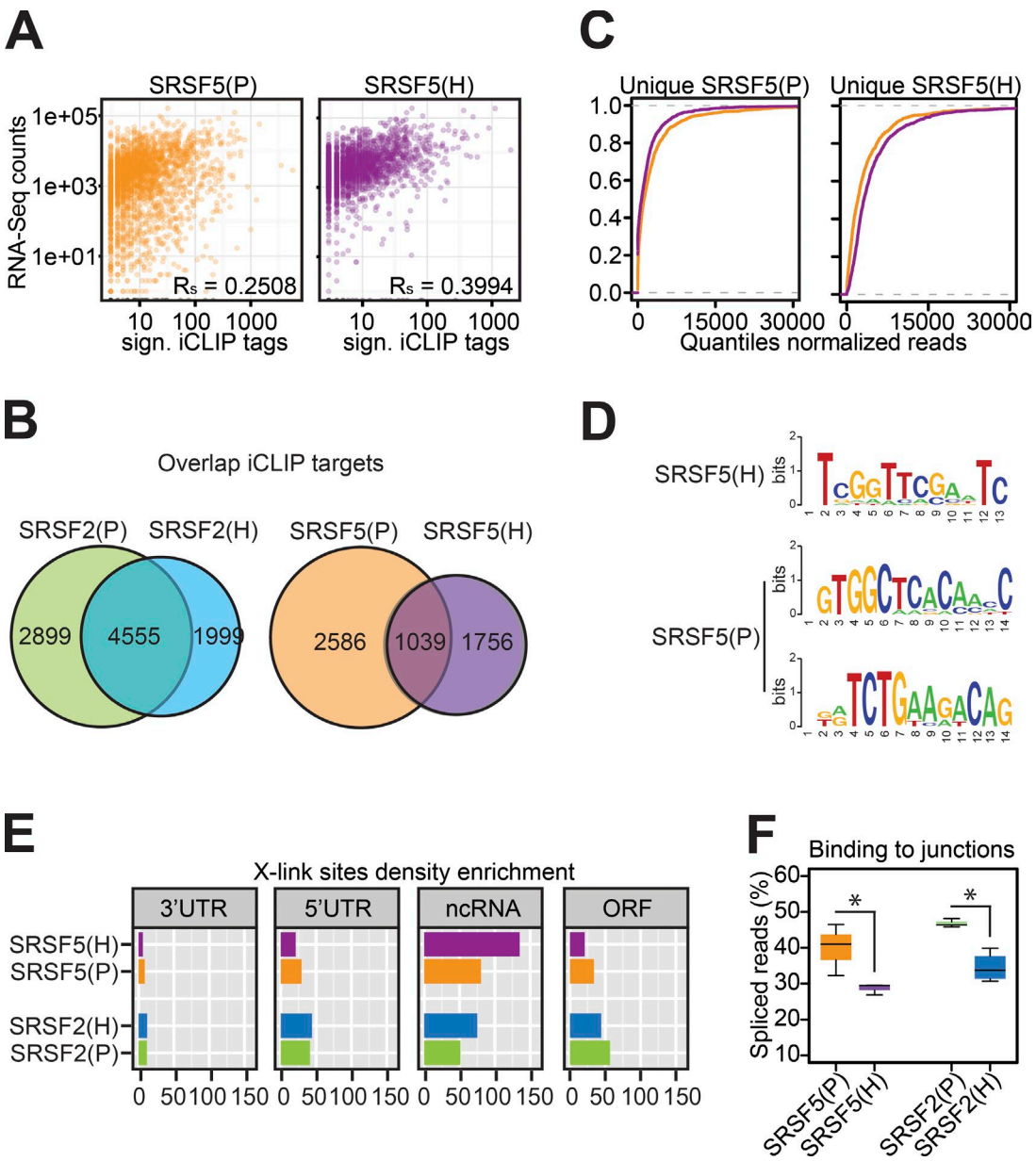

Figure 5. **SRSF5 shows differences in target binding and association with mature mRNPs.** (A) Cross-links (X-links) from replicates of SRSF2-GFP and SRSF5-GFP were pooled, normalized to similar numbers (see Table S3), and used to determine significant (sign.) binding events (iCLIP tags; FDR <0.05). iCLIP tags were plotted against normalized read counts of corresponding transcripts obtained from P19 and HeLa WT RNA-seq data (n = 2). (B) Overlap of protein-coding RNA targets (iCLIP tags >3). (C) Cumulative distribution fraction of normalized read counts (see A; n = 2) from unique P19 and HeLa targets derived in B. (D) Comparison of in vivo binding motifs of SRSF5 in P19 (P) and HeLa (H) cells. (E) Enrichment of cross-link sites of SRSF2- and SRSF5-GFP in different transcript regions normalized to input cross-link numbers and feature length. ncRNA, noncoding RNA; ORF, open reading frame. (F) Proportion of spliced versus total iCLIP reads at 5′ spice sites. *, P < 0.05 (Student's t test; n = 3).

Known splicing targets of SRSF5, such as its own mRNA (*Srsf5*), *Mcl1*, and *Cd44*, were detected in the PiCLIP data, suggesting that SRSF5 remains associated with mRNPs and may promote export and translation of its targets. To test this, we intersected SRSF5 PiCLIP targets with unique iCLIP targets and export targets (Müller-McNicoll et al., 2016). Seven genes were identified in all datasets, including *Lin28a* and *Pou5f1/Oct4*, both encoding pluripotency-specific proteins with roles in developmental timing and self-renewal (Fig. 7 C). For both transcripts, SRSF5 cross-links overlapped with NXF1 binding sites, suggesting that SRSF5 may recruit NXF1 to *Lin28a* and *Pou5f1/Oct4* for efficient export (Fig. 7 E). Accordingly, the ratios of cytoplasmic to total mRNAs decreased upon SRSF5 depletion and increased upon SRSF5 overexpression (OE), which was reflected by a slight increase in protein levels (Figs. 7, F–H; and Fig. S5 J).

SRSF5 shuttles poorly in differentiated cells

Our data indicate that shuttling of SRSF5 might be a specific trait of pluripotent cells. To confirm this, we performed shuttling assays with NIH3T3 fibroblasts stably expressing SRSF5-GFP. Indeed, SRSF5 shuttling was drastically reduced in this terminally differentiated mouse cell line (Fig. 8 A). In agreement with its proposed contribution to SRSF5 retention, SRSF2-

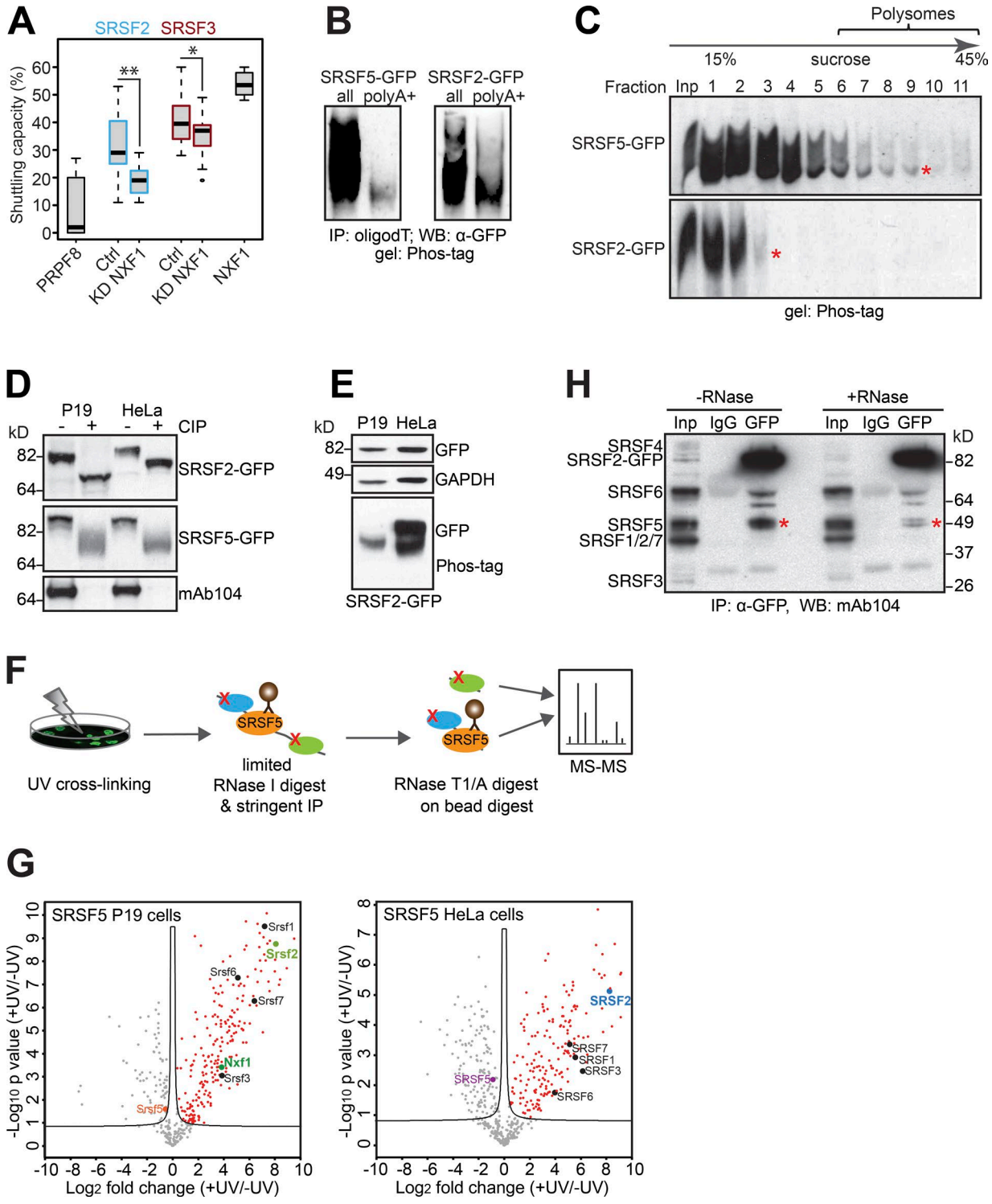

Figure 6. **Partial dephosphorylation of SRSF2 promotes shuttling of SRSF5 in P19 cells.** (A) Quantification of SRSF2- and SRSF3-GFP from 25 heterokaryons fused during NXF1 knockdown in P19 cells. *, $P < 0.01$; **, $P < 0.001$ (two-sided Wilcoxon rank-sum test). (B) Oligo(dT) capture of poly(A)+ RNA compared with input (all) followed by Phos-tag gels (40 µM) and Western blotting (WB) using anti-GFP antibodies (P19 cells). (C) Phos-tag gels (40 µM) separating sucrose gradient fractions from P19 cells followed by Western blotting using anti-GFP antibodies. Red asterisks indicate hypophosphorylated proteins. (D) P19 and HeLa lysates were incubated in calf intestinal phosphatase (CIP; 30 min) and analyzed by Western blotting using anti-GFP antibodies or mAb104 ($n = 1$). (E) SRSF2-GFP from P19 and HeLa cells was detected with anti-GFP antibodies on Phos-tag (10 µM; bottom) and normal SDS-PAGE gels (top). GAPDH served as a loading control. (F) Workflow of proximity interactome capture. MS-MS, tandem MS. (G) Volcano plot of proteins detected by tandem MS. Proteins significantly enriched in UV+ samples (red dots; FDR <0.05) for P19 ($n = 7$; left) and HeLa cells ($n = 4$; right). SR proteins and NXF1 are indicated. (H) SRSF2-GFP–bound proteins were detected after UV cross-linking and stringent IP conditions with and without RNase A treatment using mAb104 (P19 cells). Red asterisks indicate where SRSF5 copurifies with SRSF2-GFP. Inp, input.

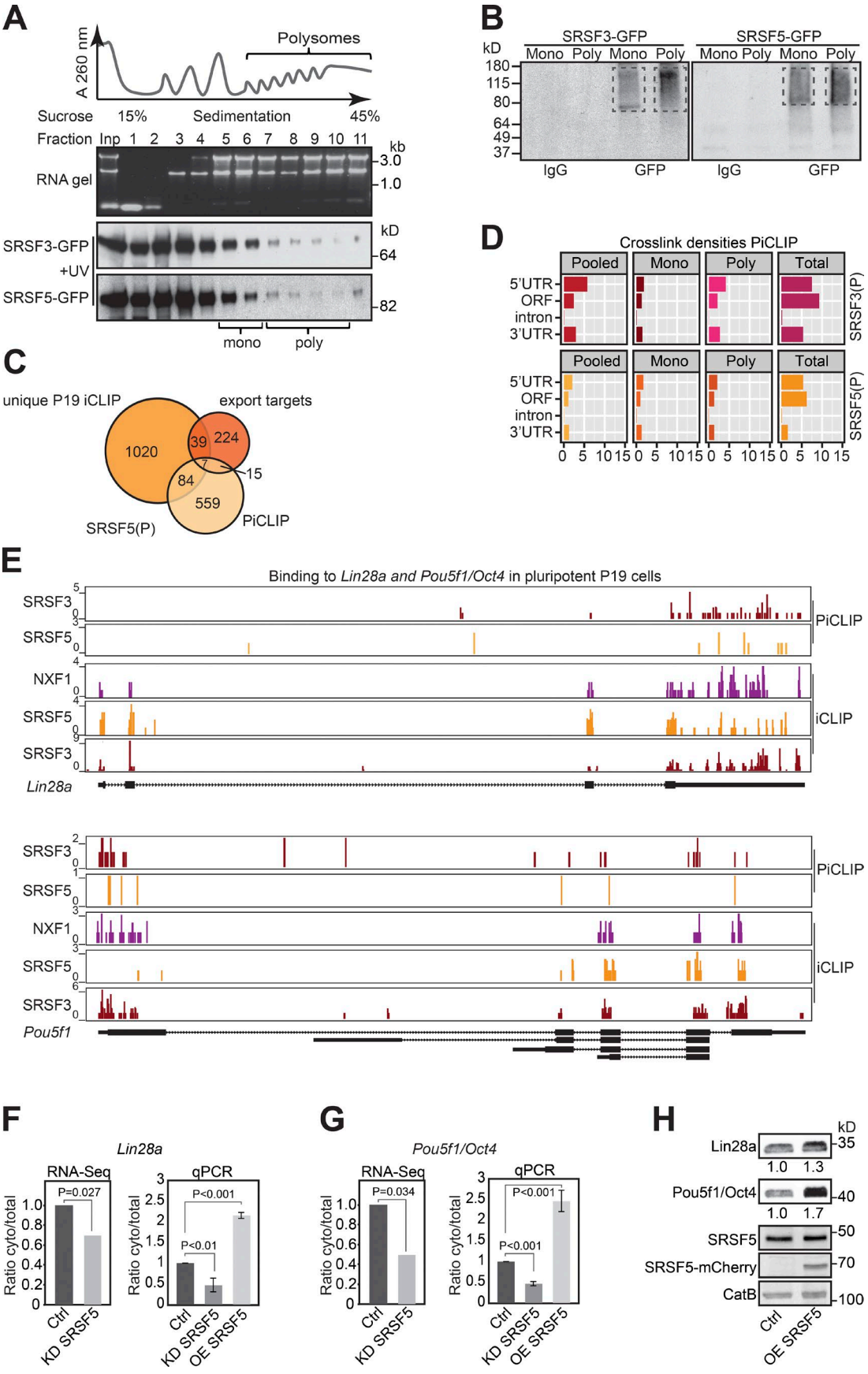

GFP was more abundant and phosphorylated in NIH3T3 cells (Fig. 8 B). To further substantiate our claim, P19 cells were differentiated into neuronal cells (Fig. 8 C; Nakayama et al., 2014), and shuttling assays were performed on day 9 of differentiation. Strikingly, shuttling of SRSF5 was significantly reduced in differentiated cells (Fig. 8 D). Moreover, the phosphorylation level of SRSF2 increased by twofold at day 8 in addition to an increase in its total level (Fig. 8 E). Altogether, these results strongly suggest that shuttling of SRSF5 is permitted in pluripotent cells but ceases when cells differentiate. This stage-specific switch in shuttling of SRSF5 may control export and retention of pluripotency-specific mRNAs.

Discussion

Although several SR proteins were reported to shuttle poorly in HeLa cells (Cáceres et al., 1998; Lin et al., 2005; Sapra et al., 2009), we have recently shown that all SR proteins act as NXF1 adapters in pluripotent P19 cells (Müller-McNicoll et al., 2016). To investigate this discrepancy, we developed a quantitative shuttling assay to measure the nucleocytoplasmic shuttling of seven canonical family members. Key technical advances were the use of stable clonal cell lines expressing similar and near-endogenous levels of GFP-tagged proteins (donor) and a membrane-bound marker protein (recipient). Quantification of total nuclear fluorescence in a large number of donor and recipient cells allowed for the first time the determination of mean shuttling capacities of individual SR proteins. We could show that all seven SR proteins shuttle in P19 cells; however, they shuttle to different extents, suggesting a differential participation in nuclear export and retention of mRNAs. SR proteins were sorted into three shuttling groups, which correlated well with their numbers of export targets, their RNA-binding preferences (Müller-McNicoll et al., 2016), their numbers of potential phosphorylation sites, their extent of NXF1 interaction, and their presence in cytoplasmic fractions. Altogether, we present a novel quantitative assay that enables robust quantifications of nucleocytoplasmic shuttling. Our assay is broadly applicable to the quantification of differences in the shuttling capacities of RBPs in different cellular conditions, to study mutants or knockout cell lines, and to test the effect of inhibitors, which was not possible thus far.

We discovered that SRSF2 and SRSF5 shuttle in pluripotent P19 cells but not in HeLa cells. In agreement with this, SRSF5 is exclusively present in cytoplasmic fractions containing polysomes and in NXF1-containing mRNPs in P19 cells. Thus, SRSF2 and SRSF5 are not strictly nonshuttling SR proteins as suggested from studies using HeLa cells (Cáceres et al., 1998; Sapra et al., 2009). SRSF2 and SRSF5 also shuttle poorly in MEFs, which are not pluripotent (Lin et al., 2005), and more importantly, shuttling is also reduced in differentiated P19 cells. Thus, our data argue for cell state–specific rather than species-specific differences in shuttling. They further imply that shuttling of SRSF5 and possibly other RBPs is regulated in different cell types, presumably to control export, localization, and translation of specific transcripts. We propose that SRSF5 undergoes a shuttling switch during differentiation. A similar switch might also occur during cellular stress, oncogenic transformation, or viral infection, which could explain the contradictory observation that SRSF5 promotes the translation of viral transcripts in infected HeLa cells (Swanson et al., 2010). So far, SRSF5 has been poorly studied, despite being an emerging marker for several cancer types (Kim et al., 2016). The cell type– and state–specific differences in nucleocytoplasmic shuttling of SR protein family members observed herein underline the importance of the cellular context for the function of these and other multifunctional RBPs.

Our data suggest that shuttling of SRSF2 and SRSF5 is independent of the primary protein sequence. Instead, differential PTMs, such as arginine methylation and serine phosphorylation, may modulate shuttling. In P19 cells, arginine residues flanking the NXF1 interaction region were more dimethylated and are shown here to be important for NXF1 interaction and shuttling. Similarly, THOC5 and CHTOP, two other NXF1 export adapters, require arginine methylation for NXF1 interaction (Chang et al., 2013). Moreover, methylation of arginine residues within the NXF1 interaction domain of SRSF1 regulates its cytoplasmic abundance (Sinha et al., 2010); however, those residues are not homologous to the arginines identified in our study. A recent methylome study in human HEK293 cells identified methylated R_{86} and R_{92} in SRSF5, but also did not detect methylation on R_{93} (Larsen et al., 2016). Interestingly, R_{92} methylation decreased upon knockdown of the methyltransferase PRMT1 (Larsen et al., 2016). PRMT1 was also enriched in the SRSF5 proximity interactomes, confirmed by coIP (unpublished data), suggesting that PRMT1 might be responsible for the methylation of R_{86} and R_{92} in SRSF5. Arginine methylations also influence the RNA-binding capacities of RBPs; ALYREF showed reduced RNA binding, and SFPQ showed enhanced binding to RNA when arginine residues were methylated (Hung et al., 2010; Snijders et al., 2015). We noted that RRM2 of SRSF5, which cross-linked substantially more to RNA in pluripotent P19 cells, had slightly higher arginine methylation levels.

It was previously shown that nucleocytoplasmic shuttling of hnRNPA1 is regulated during stress conditions through phosphorylation by p38 kinase, which regulates its availability for splicing (van der Houven van Oordt et al., 2000). We show here that phosphorylation of SRSF5 itself was not altered; instead, phosphorylation of cobound SRSF2 affected the shuttling properties of the entire SRSF5-containing mRNP. This indicates that mRNP functionality can also be controlled by modifications on

Figure 7. **SRSF5 binds to pluripotency-specific transcripts in polysomal fractions and affects their nucleocytoplasmic distribution.** (A) Polysome profile of P19 cells after UV cross-linking. Indicated fractions were pooled to obtain monosomal (5 and 6; Mono) and polysomal (7–10; Poly) fractions. Inp, input. (B) Protein–RNA complexes immunopurified from pooled fractions using anti-GFP or nonspecific antibodies (IgG). Boxed areas indicate cut regions. (C) Overlap of RNA targets identified by PiCLIP, unique targets from total iCLIP, and export targets of SRSF5 (Müller-McNicoll et al., 2016). (D) Comparison of cross-link densities (FDR <0.05) from PiCLIP (monosomal, polysomal, or pooled) to total iCLIP data (Total) in different transcript regions normalized to feature length. ORF, open reading frame. (E) Significant cross-link events in *Lin28a* and *Pou5f1/Oct4* from total iCLIP and PiCLIP for SRSF3-GFP (dark red), SRSF5-GFP (orange), and NXF1-GFP (purple; Müller-McNicoll et al., 2016). (F and G) Ratios of cytoplasmic (cyto) to total *Lin28a* (F) and *Pou5f1/Oct4* (G) transcript abundance after SRSF5 knockdown (KD) or OE quantified by RNA-seq (left; $n = 2$) and reverse transcription quantitative PCR (qPCR; right; $n = 4$). Error bars indicate SD. (H) Western blotting for Lin28a and Pou5f1/Oct4 proteins upon SRSF5 OE. Quantifications of signal relative to control (Ctrl) are shown below each blot. β-Catenin (CatB) served as a loading control.

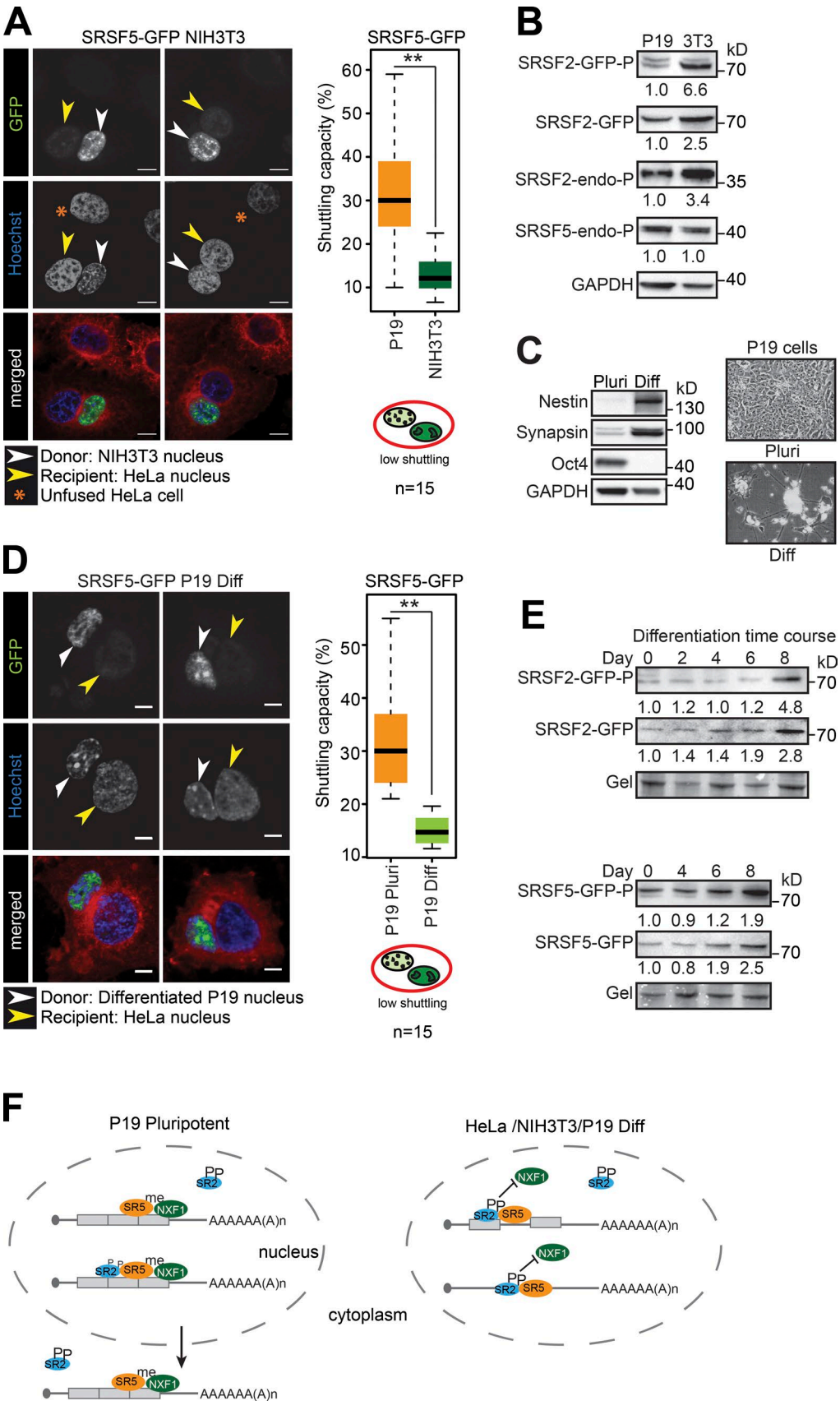

Figure 8. **SRSF5 shuttles poorly in differentiated cells.** (A, left) Two representative fusion events of NIH3T3 cells expressing SRSF5-GFP (donor) and HeLa cells expressing CAAX-mCherry (recipient). (Right) Quantification from 15 heterokaryons. (B) Western blotting analysis of total and phosphorylated SRSF2 (SR2; GFP-tagged and endogenous [endo]) using anti-GFP or mAb104 antibodies. GAPDH served as a loading control. (C, left) Western blotting analysis

frequent interaction partners. In agreement with a phosphoproteome study performed during differentiation of mouse embryonic stem cells (Rigbolt et al., 2011), we observed that the phosphorylation level of SRSF2 increases in P19 cells upon differentiation. So far, little is known about how PTMs impact on RNA binding, the splicing outcome, and shuttling of SR proteins. Our data support the notion that mRNP dynamics are posttranslationally regulated to allow rapid changes in the binding of RNA, protein partners, or coregulators as a means to integrate signaling pathways when cellular conditions change, such as during differentiation of pluripotent cells.

SRSF2 harbors an NRS in its RS domain, conferring phosphatase resistance (Cazalla et al., 2002). Consequently, SRSF2 remains phosphorylated after splicing, is unable to recruit NXF1 in HeLa and fibroblast cells, and is sorted away from shuttling mRNPs (Lin et al., 2005). SRSF5, however, does not contain an NRS, and its shuttling disability in HeLa cells was not understood. Our data indicate that SRSF2 is highly enriched in SRSF5-containing mRNPs and that both proteins share 90% of their RNA targets and binding sites in exons. In pluripotent P19 cells, SRSF2 is dephosphorylated during splicing and appears in NXF1-containing mRNPs. In agreement with shuttling, SRSF2-GFP accumulates in the cytoplasm when reimport is blocked by ActD or by knockdown of TRN-SR2 (unpublished data). However, SRSF2 does not bind NXF1 directly and is excluded from polysomal fractions, suggesting that it shuttles passively and is rapidly removed from mRNPs after export. Partial dephosphorylation of cobound SRSF2 may allow recruitment of NXF1 to the mRNP via SRSF5, and both proteins may shuttle together with bound RNA to the cytoplasm, with SRSF2 being a passive passenger. In HeLa cells, however, SRSF2 is phosphatase-resistant and excluded from NXF1-containing mRNPs, in line with a previous study (Fig. 8 F; Cazalla et al., 2002).

Structural in vitro studies showed that mRNAs bound by SR proteins are handed over to NXF1 before mRNA export, suggesting that SR proteins remain a passive part of the shuttling mRNP (Hargous et al., 2006; Tintaru et al., 2007). However, in vivo studies suggest that SR proteins remain bound to alternatively spliced transcripts, recruit NXF1, and accompany the transcripts to the cytoplasm to regulate their translation (Maslon et al., 2014; Müller-McNicoll et al., 2016). To address this, we developed iCLIP from polysomal fractions (PiCLIP), which enabled for the first time the identification of transcripts bound by SRSF3 and SRSF5 in cytoplasmic polysomal fractions and confirmed that some mRNAs undergoing translation are directly bound to SR proteins. Preferential detection in 3′ UTRs indicates that SR proteins are removed from coding regions by translating ribosomes, but they persist in 3′ UTRs. The low proportion of SR proteins cosedimenting with ribosomes suggest that the vast majority are rapidly rephosphorylated after export and dissociate from the mRNP; however, a subset of shuttling SR proteins, including SRSF5, escape mRNP remodeling and deliver their mRNA cargo to the ribosome, possibly to regulate its expression.

Our iCLIP data indicate that both RRMs of SRSF5 participate in RNA binding. Their differential contribution suggests that RRM2 accessibility might be regulated in different cell types, which would help to coordinate the binding of cell type–specific RNA targets. Occupation of RRM2 with RNA may also protect SRSF5 from rephosphorylation by SRPK1 in the cytoplasm and prevent its removal from the mRNP because the binding sites of SRPK1 and RNA on RRM2 are overlapping (Tintaru et al., 2007).

In conclusion, SRSF5 affects the nuclear export of pluripotency-specific transcripts, shuttles to the cytoplasm, and remains bound to spliced mRNA targets in polysomal fractions, suggesting that SRSF5 performs specific functions in pluripotent P19 cells. In differentiated P19 cells, HeLa cells, and NIH3T3 cells, SRSF5 shuttling does not occur, possibly because RNA targets are not expressed or are retained in the nucleus. PTMs such as arginine methylation and serine phosphorylation may control a switch between shuttling and nuclear retention of SRSF5, which allows the same protein to perform different functions in changing cellular conditions, e.g., promoting the retention of pluripotency-specific mRNAs at the onset of differentiation, which might help to fine-tune the regulation of gene expression and cell fate. Regulated shuttling could control the nuclear availability of splicing factors and their cytoplasmic activities by rapidly responding to changing cellular conditions. Exploration of nuclear retention and shuttling as means to control gene expression is still at the beginning, and the assays and methods developed in this study will undoubtedly be useful to this emerging field.

Materials and methods

Generation of stable BAC cell lines

BACs harboring the SR proteins NXF1 and PRPF8 from mouse or human origin were GFP-tagged by BAC recombineering as described previously (Poser et al., 2008). Mouse SRSF3 and SRSF5 BACs were further mutated by BAC recombineering according to Wang et al. (2014) to introduce point mutations. BAC DNA was isolated from *Escherichia coli* DH10 cells using a BAC prep kit (MACHEREY-NAGEL). P19 and HeLa cells were grown in DMEM Glutamax medium (Gibco) supplemented with 10% heat-inactivated FBS (Gibco), 100 U/ml penicillin, and 100 µg/ml streptomycin (PenStrep; Gibco) on cell culture dishes coated with 0.1% gelatin (Sigma-Aldrich) under humidified 5% CO_2 at 37°C. P19 and HeLa WT cells were transfected with 1 µg BAC DNA using Effectene (QIAGEN), and stable clonal cell lines were obtained after selection with 500 µg/ml geneticin (Gibco) and FACS sorting. The CAAX-mCherry plasmid (TH0477) was stably integrated into HeLa WT cells and selected with 0.5 µg/ml puromycin (Sigma-Aldrich).

Quantitative shuttling assay

Approximately 4×10^5 cells (each P19 and HeLa CAAX-mCherry or reverse) were seeded together on coverslips and cocultured overnight in DMEM. Cells were incubated with 50 µg/ml CHX (Sigma-Aldrich) or 0.5 µg/ml puromycin (Puro; Gibco) for 2 h followed by 100 µg/ml

of pluripotent (Pluri) and differentiated (Diff) P19 cells using antibodies specific for Oct4 and the neuronal differentiation markers synapsin and nestin. (Right) Neurite outgrowth in differentiated P19 cells. (D, left) Two representative fusion events of P19 cells expressing SRSF5-GFP at day 9 of differentiation. (Right) Quantification of 15 heterokaryons. **, $P < 0.001$ (two-sided Wilcoxon rank-sum test). Bars, 10 µm. (E) Time course of P19 cells differentiating into neuronal cells (day 0 to day 8; $n = 2$). (F) Model of cell state–specific shuttling capacities of SRSF5 (SR5). In pluripotent cells, SRSF5 stably recruits NXF1 to the mRNPs because of higher methylation levels of arginine residues important for NXF1 interaction and also because of partial dephosphorylation of SRSF2, which binds in proximity to SRSF5 on many mRNAs. In differentiated cells, either SRSF5 binds more noncoding RNAs or bound mRNAs are not efficiently exported to the cytoplasm because of lower methylation levels of SRSF5 and because of phosphatase resistance of SRSF2.

CHX or 1 µg/ml Puro for 30 min to block protein synthesis. Cell fusion was achieved by incubation with 50% PEG1500 (Roche) for 2 min. Fused cells were further grown in the presence of 100 µg/ml CHX or 1 µg/ml Puro for 3 h. Cells were fixed with 4% PFA and either stained with 6 µg/ml Hoechst 33258 (Sigma-Aldrich) and mounted with DABCO (Sigma-Aldrich) or stained with 0.25 µg/ml Hoechst 34580 (Sigma-Aldrich) and mounted with Prolong Diamond Antifade Mountant (Thermo Fisher Scientific). As an alternative test for shuttling, P19 cells stably expressing SRSF2-GFP and SRSF5-GFP were treated with 5 µg/ml actinomycin D (ActD), to inhibit transcription by RNA Pol II, and 20 µg/ml CHX, to block de novo protein synthesis, for 3 h. Cells were fixed and stained with Hoechst before imaging.

Microscope image acquisition

Images were acquired as 0.3 µm z stacks using a DeltaVision microscope (Applied Precision Ltd.) or a confocal laser-scanning microscope (LSM780; ZEISS) with a Plan-Apochromat 63× 1.4 NA oil differential interference contrast objective equipped with two photomultiplier tubes and a gallium arsenite phosphate (GaAsP-PMT) detector system. SoftWoRx software (GE Healthcare) was used for acquisition and deconvolution (Applied Precision Ltd.) of images acquired with the DeltaVision microscope, and ZEN 2012 (black edition; 8.0.5.273; ZEI SS) was used for acquisition of images with the LSM780 microscope. Deconvolved images were processed and analyzed with FIJI (ImageJ; National Institutes of Health).

Quantification of shuttling capacities

To quantify GFP signals in heterokaryons, z stacks spanning both nuclei of a heterokaryon from top to bottom were projected, and pixel values were summed. Nuclei of fused cells plus one nucleus of an unfused HeLa cell in the same image were encircled, and the sum of the GFP values of all pixels of one nucleus was measured as fluorescence intensity per nucleus. Fluorescence intensities of unfused cell nuclei divided by their area served as a value for background fluorescence, which was subtracted from the fluorescence intensities of nuclei of the respective heterokaryon. Obtained total GFP intensities of both nuclei within a heterokaryon were used to calculate the fluorescence fractions attributable to donor and recipient nuclei.

Polysome profiling

Approximately 2×10^7 P19 cells were treated with 100 µg/ml CHX for 10 min to stabilize translating ribosomes and subsequently were harvested by trypsination (Gibco). Cell extracts were fractionated over linear 15–45% sucrose density gradients (prepared in 10 mM Hepes, pH 7.2, 150 mM KCH_3CO_2, and 5 mM $MgCl_2$) by centrifugation at 270,000 *g* for 120 min. Fractions (1 ml each) were collected from the top to the bottom of the gradient and analyzed for absorption at 260 nm and on RNA gels. For RNA analysis, 300 µl of each fraction was extracted with TRIzol (Thermo Fisher Scientific) and separated on 1.5% agarose gels. For protein analysis, 20 µl of each fraction were mixed with 5× Laemmli buffer, separated on a 4–12% NuPAGE gradient gel (Thermo Fisher Scientific), and analyzed by Western blotting.

CoIP and Western blotting

Approximately 5×10^7 cells were lysed in NET-2 buffer supplemented with 1× complete protease inhibitor cocktail (Roche) and 10 mM β-glycerophosphate (Fluka BioChemica) and sonicated for 30 s at a 20% amplitude (Branson W-450 D; Thermo Fisher Scientific). Cleared cell lysates were exposed to 100 µg/ml RNase A or left without and then were incubated for 20 min at 23°C. 0.2% of lysate served as input. 10 µg of goat IgG (Sigma-Aldrich) or goat α-GFP (provided by D. Drechsel, Max Planck Institute of Molecular Cell Biology and Genetics, Dresden, Germany) was preincubated with Gamma Bind sepharose beads (GE Healthcare) for 1 h at 4°C and then was mixed with equal amounts of untreated or RNase A–treated lysates for 1.5 h at 4°C. Beads were washed, and cobound proteins were eluted with 2× Laemmli buffer. For Western blotting, proteins were resolved on 4–12% NuPAGE gradient gels (Thermo Fisher Scientific), blotted on nylon membranes (EMD Millipore), and probed with the following antibodies: goat α-GFP, goat α-NXF1 (Santa Cruz Biotechnology, Inc.), rabbit α-PABPN1 (Abcam), mouse α-SRPK1 (BD), mouse α-RP6 (BD), mouse α-GAPDH (Santa Cruz Biotechnology, Inc.), mouse mAb104 (CRL_2067; ATCC), rabbit α-Lin28a (Cell Signaling Technology), rabbit α-SRSF5 (EMD Millipore), rabbit α-Beta catenin (Abcam), rabbit α-Oct4 (Abcam), mouse α-nestin (Santa Cruz Biotechnology, Inc.), rabbit α-synapsin (Cell Signaling Technology), and mouse α-TNPO3 (Abcam). Quantification was done using FIJI, and values were normalized to the controls.

Oligo(dT) capture and phosphorylation status of SR proteins

To analyze the phosphorylation status of SR proteins bound to polyadenylated mRNAs, $\sim 2 \times 10^7$ cells grown at 90% confluency were irradiated twice with 0.25 J/cm^2 UV light at 254 nm on ice. Cells were harvested and lysed, and DNA was sheared by passing the lysate 20 times through a 20 G needle. 0.2% of lysate served as input. Poly(A)$^+$ mRNAs and cross-linked proteins were captured on oligo$(dT)_{25}$ magnetic beads (three rounds of 1 h at 4°C; S1550S; New England Biolabs, Inc.). After each round, oligo$(dT)_{25}$ beads were washed with wash buffers I–III that contained decreasing concentrations of LiCl and LiDS according to the manufacturer's instructions (New England Biolabs, Inc.). Cross-linked proteins were eluted in 150 µl elution buffer at 55°C for 5 min and precipitated overnight in 10% TCA. Pellets were washed with ice-cold acetone and resuspended in 2× Laemmli buffer. Proteins were separated on 6% acrylamide gels (29:1; Bio-Rad Laboratories) containing 40 µM Phos-tag (Wako Pure Chemical Industries). Gels were treated according to the manufacturer's instructions before transfer to a nitrocellulose membrane, and phosphorylated SR proteins were subsequently analyzed by Western blotting using goat anti-GFP antibodies.

iCLIP and RNA-seq library preparation

HeLa BAC cells were irradiated once with 150 mJ/cm^2 UV light (254 nm), and iCLIP was performed as described previously (Änkö et al., 2012; Müller-McNicoll et al., 2016). Protein G DynaBeads (Thermo Fisher Scientific) coupled with goat anti-GFP antibody (provided by D. Drechsel) were used for IP. Cross-linked immunopurified RNA was digested to lengths of 60–150 nucleotides, reverse transcribed to generate cDNA libraries, and subjected to high-throughput sequencing on a HiSeq2000 machine (single-end 75 nucleotide reads; Illumina). Use of the same antibody, identical conditions, and parallel library preparation permitted a direct comparison among the P19 and HeLa datasets. Total RNA was isolated from HeLa and P19 WT (two replicates) and sequenced after rRNA depletion (RiboMinus) on a HiSeq2000 machine (single-end 75 nucleotide reads).

Analysis of iCLIP and RNA-seq data

Adapters and barcodes were removed from all iCLIP reads before mapping to the mouse mm9 genome assembly (Ensembl59 annotation) using Bowtie software (version 0.10.1). To determine statistically significant cross-link sites, uniquely mapping reads were used, and cross-links were extracted and randomized within cotranscribed regions. Significant binding events (iCLIP tags; false discovery rate [FDR] <0.05) were calculated using normalized numbers of input cross-link sites as previously described (Yeo et al., 2009; König et al., 2010; Wang et al., 2010). To obtain comparable numbers of significant binding sites for SRSF2 and SRSF5, replicates that correlated well were pooled.

For exon cobinding, all exons were compiled, and the number of significant binding sites for each SR protein was counted in these features. Exons without iCLIP reads were removed, the percentage of cobound exons compared with all bound exons was calculated for each SR protein, and hierarchical clustering using distance correlation was performed.

For motif searching, a z score analysis for enriched k-mers was performed as described previously (Wang et al., 2010). Sequences surrounding significant cross-links were extended in both directions by 30 nucleotides to exclude the conserved AG nucleotides at 3′ splice sites (windows: −30 to −5 nt and 5–30 nt relative to the 3′ splice site). Uniquely occurring k-mers within the evaluated interval were counted and weighted by 1.0. A reference dataset was generated by 100× randomly shuffling significant cross-links within the same genes, and a z score was calculated relative to the randomized genomic positions. The top 15 k-mers were used to determine the in vivo binding consensus motif. Enriched octamers were analyzed, and 10 nt around the binding sites were excluded from the analysis to avoid any bias caused by differences in the cross-linking efficiency of different nucleotides.

To quantify the ratio of spliced and unspliced RNAs bound to SRSF2 and SRSF5 from P19 and HeLa cells, iCLIP reads from three or four replicates were trimmed and mapped to the mm10 or hg38 genome assembly using Spliced Alignment to a Reference (STAR) software (Dobin et al., 2013). Annotated 5′ splice sites (mm10 or hg38) were compiled and intersected with mapped iCLIP reads (window ± 50 nt). Only reads that had at least 3 nt overhang across exon borders were considered. All iCLIP reads that mapped to the 5′ splice site and continued from one exon into the neighboring intron were counted as unspliced, and reads that spanned two neighboring exons were counted as spliced. 5′ splice sites were chosen because SR proteins bind close to 5′ splice sites, and the iCLIP reads started at the cross-link sites owing to the library prep.

RNA-seq reads were trimmed and mapped to the mm10 and hg38 genome assemblies, respectively, using STAR (Dobin et al., 2013), counted using htSeq, and normalized to library depth using DESeq2 (Love et al., 2014).

Sample preparation and MS

HeLa and P19 cells expressing SRSF5-GFP were irradiated twice with 250 mJ/cm^2 UV light (254 nm) on ice. Cells without UV irradiation were used as UV$^-$ controls. Cell lysates were treated with DNase I (Ambion), sonicated mildly, and incubated with RNase I (Ambion) for exactly 5 min at 37°C to partially digest the RNA, identical to iCLIP conditions (Huppertz et al., 2014). Resulting RNA fragments were on average 100 nt long. Absence of PABPN1 and PABPC binding was used to control for the limited RNA digestion. SRSF5-GFP protein was immunopurified using anti-GFP antibodies on magnetic beads under high-salt conditions (1 M NaCl). Subsequently, beads were washed (50 mM ammonium bicarbonate), and proteins binding to SRSF5 via cross-linked RNA were eluted by digestion with 30 ng/µl RNase T1 and 0.2 ng/µl RNase A on beads for 30 min at 52°C. Eluted proteins and proteins remaining on the beads were digested with 500 ng trypsin/LysC (Promega) in 50 mM ammonium bicarbonate. To capture longer peptides from the RS region of SRSF5-GFP, aliquots of 10 µl digestion mixture were taken after 5, 10, and 30 min and were stopped with formic acid (FA) at 1% final concentration. Partial digestion aliquots were combined with the completely digested samples and analyzed either by direct injection to liquid chromatography (LC)/tandem MS or after purification on stage tips (Rappsilber et al., 2007). Phosphorylated and cross-linked peptides were additionally enriched using TiO_2 beads (GL Science Japan; Larsen et al., 2005) with modification according to Richter et al. (2009).

LC/MS was performed on a QExactive Plus equipped with an ultra-high performance LC unit (Dionex Ultimate 3000) and a Nanospray Flex Ion-Source (Thermo Fisher Scientific). Peptides were loaded on a C18 reverse-phase precolumn (Thermo Fisher Scientific) followed by separation on an in-house packed picotip emitter (2.4 µm Reprosil C18 resin; Dr. Maisch GmbH; diameter 100 µm and 15 cm long; New Objectives) using a gradient from mobile phase A (4% acetonitrile and 0.1% FA) to 30% mobile phase B (80% acetonitrile and 0.1% FA) for 20 min followed by a second gradient until 60% B for 10 min with a flow rate of 400 nl/min and washout with 99% B for 5 min. MS data were recorded by a data-dependent acquisition Top10 method selecting the most abundant precursor ions in positive mode for higher-energy collisional dissociation fragmentation. The full MS scan range was 300–2,000 m/z with resolution of 70,000 and an automatic gain control value of 3×10^6 total ion counts with a maximal ion injection time of 160 ms. Only higher charged ions (≥2) were selected for tandem MS scans with a resolution of 17,500, an isolation window of 2 m/z, and an automatic gain control value set to 10^5 ions with a maximal ion injection time of 150 ms. The first mass was fixed to 110 m/z. Selected ions were excluded in a time frame of 30 s after the fragmentation event. Data were acquired in profile mode.

MS data analysis

Data were analyzed using MaxQuant (v1.5.3.30; Cox and Mann, 2008). Proteins were identified using the reference proteome database UniProtKB for mice (released in June 2015; 76,086 entries) and humans (released in June 2015; 68,508 entries) supplemented with the sequence of the SRSF5-GFP isoforms. The enzyme specificity was set to trypsin, missed cleavages were limited to two, and the minimum peptide length was seven amino acids. Acetylation (+42.01) at the N terminus and oxidation of methionine (+15.99) were selected as variable modifications, and carbamidomethylation (+57.02) was selected as fixed modification on cysteines. The FDR for the identification protein and peptides was 1%.

LFQ was recorded with at least one peptide. Identifications from the reverse decoy database were done by site, and known contaminants were excluded. Data were further analyzed by Perseus 1.5.2.6 (Cox and Mann, 2012). Proteins were quality filtered according to a minimum of six valid values in one group (P19; $n = 7$) or three valid values in one group (HeLa; $n = 4$). All missing values from this reduced matrix were replaced by background values from normal distribution. For statistical comparison, permutation-based FDR and Student's t test were used. Proteins were considered if they were significantly enriched in UV-treated samples (FDR >0.05).

PTMs were identified by PEAKS 7.0 proteomics software (Bio-Informatics Solutions Inc.). Quantifications were performed by spectral counting for site-specific quantifications or by LFQ quantification of the single fractions to compare the UV$^+$ and UV$^-$ fractions from both species. Parent ion mass accuracy was set to 10 ppm, and the fragment ion mass accuracy was set to 0.02 D. Up to four missed cleavages and a maximum of two PTMs per peptide were allowed. Monooxidation (+15.99) at CMFPYWH, dioxidations (+31.97) at CMFPYW, phosphorylation (+79.97) at STY, mono- (+14.02), di- (+28.03), and tri-methylation (+42.05) at KR, and acetylation (+42.01) at TSCYH were included in the search.

All cross-linked fractions were screened for peptide:RNA cross-link spectra essentially as described by Richter et al. (2009). Spectra that showed marker ions of RNA-specific fractions (nucleobases: A: = 136, G: = 152, C: = 112, and U: = 113) were further investigated for a good peptide sequence coverage, and if present, de novo sequencing of the peptide fragments was performed. Extracted ion chromatograms were used to quantify best peptide-RNA cross-link features. Quantified

peaks were matched manually by retention times, m/z, and calculated ratios of peak areas for P19/HeLa cells.

Knockdowns and RNA isolation

To produce customized endoribonuclease-prepared siRNAs (esiRNAs), two suitable regions of ∼400 bp were chosen for mouse *Nxf1* and *Srsf5* using the DEQOR2 suite (Surendranath et al., 2013). Forward and reverse primers were designed, each containing the T7-promoter sequence at the 5′ end. Amplified esiRNA target regions were in vitro transcribed (Megascript T7 kit; Ambion) to produce double-stranded RNA, which was subsequently digested to small fragments of 18–25-bp length by RNase III (provided by D. Drechsel) and purified. For knockdowns, 5×10^4 P19 cells were seeded in six-well plates and then grown until 25% confluency, and 2 µg esiRNA were transfected per well using Lipofectamine 2000 (Thermo Fisher Scientific). An esiRNA against GFP was used as a control. To reduce secondary effects of protein knockdown, esiRNA transfections were kept short (24 h for NXF1 and 36 h for SRSF5). Cells were harvested, and RNA was isolated using TRIzol (Thermo Fisher Scientific).

Online supplemental material

Fig. S1 shows the development of a quantitative shuttling assay for SR proteins in pluripotent P19 cells. Fig. S2 shows shuttling correlations and controls. Fig. S3 shows how methylation of arginine residues within the NXF1 interaction region affects SRSF5 shuttling. Fig. S4 shows our experiments with RNA cross-links and iCLIP to compare RNA binding specificities of SRSF5 in P19 and HeLa cells. Fig. S5 shows how SRSF2 and SRSF5 bind in close proximity on the same RNA. Table S1 shows how pairwise comparisons of shuttling capacities reveal distinct shuttling groups. Table S2 shows replicate correlations of iCLIP experiments. Table S3 shows iCLIP mapping statistics. Table S4 shows interactors binding in close proximity to SRSF5-GFP in P19 cells (RNase-sensitive). Table S5 shows interactors binding in close proximity to SRSF5-GFP in P19 cells (partially RNase-resistant). Table S6 shows interactors binding in close proximity to SRSF5-GFP in HeLa cells (RNase-sensitive). Table S7 shows interactors binding in close proximity to SRSF5-GFP in HeLa cells (partially RNase-resistant).

Acknowledgments

We thank A. Dahl for advice and sequencing of RNA-seq and iCLIP libraries, C. Kowatsch for help with some iCLIP libraries, M. Köhn for advice on polysome profiling, H. Schewe for support on confocal microscopes, S. Schulze-Dramac for technical assistance, and M. Brugiolo, J. Wöhnert, A. Cléry, and F. Allain for helpful discussions.

We are grateful for funding from the Deutsche Forschungsgemeinschaft to K. Zarnack (FOR2333 and SFB902), K.M. Neugebauer (NE909/3-1) and to M. Müller-McNicoll (CEF-MC and SFB902).

The authors declare no competing financial interests.

Author contributions: V. Botti, M.C. Steiner, A. Solovyeva, F.M. Richter, F. McNicoll, M. Wegener, O.D. Schwich, and M. Müller-McNicoll performed the experiments. M.C. Steiner, F. McNicoll, F.M. Richter, I. Wittig, K. Zarnack, and M. Müller-McNicoll performed the analyses. I. Poser contributed reagents and advice. M.C. Steiner, F. McNicoll, F.M. Richter, and M. Müller-McNicoll prepared the figures. The manuscript was written by K. Zarnack, K.M. Neugebauer, and M. Müller-McNicoll.

Submitted: 15 October 2016
Revised: 22 March 2017
Accepted: 24 April 2017

References

Änkö, M.L. 2014. Regulation of gene expression programmes by serine-arginine rich splicing factors. *Semin. Cell Dev. Biol.* 32:11–21. http://dx.doi.org/10.1016/j.semcdb.2014.03.011

Änkö, M.L., L. Morales, I. Henry, A. Beyer, and K.M. Neugebauer. 2010. Global analysis reveals SRp20- and SRp75-specific mRNPs in cycling and neural cells. *Nat. Struct. Mol. Biol.* 17:962–970. http://dx.doi.org/10.1038/nsmb.1862

Änkö, M.L., M. Müller-McNicoll, H. Brandl, T. Curk, C. Gorup, I. Henry, J. Ule, and K.M. Neugebauer. 2012. The RNA-binding landscapes of two SR proteins reveal unique functions and binding to diverse RNA classes. *Genome Biol.* 13:R17. http://dx.doi.org/10.1186/gb-2012-13-3-r17

Aubol, B.E., R.M. Plocinik, J.C. Hagopian, C.T. Ma, M.L. McGlone, R. Bandyopadhyay, X.D. Fu, and J.A. Adams. 2013. Partitioning RS domain phosphorylation in an SR protein through the CLK and SRPK protein kinases. *J. Mol. Biol.* 425:2894–2909. http://dx.doi.org/10.1016/j.jmb.2013.05.013

Borer, R.A., C.F. Lehner, H.M. Eppenberger, and E.A. Nigg. 1989. Major nucleolar proteins shuttle between nucleus and cytoplasm. *Cell.* 56:379–390. http://dx.doi.org/10.1016/0092-8674(89)90241-9

Cáceres, J.F., G.R. Screaton, and A.R. Krainer. 1998. A specific subset of SR proteins shuttles continuously between the nucleus and the cytoplasm. *Genes Dev.* 12:55–66. http://dx.doi.org/10.1101/gad.12.1.55

Cazalla, D., J. Zhu, L. Manche, E. Huber, A.R. Krainer, and J.F. Cáceres. 2002. Nuclear export and retention signals in the RS domain of SR proteins. *Mol. Cell. Biol.* 22:6871–6882. http://dx.doi.org/10.1128/MCB.22.19.6871-6882.2002

Chang, C.T., G.M. Hautbergue, M.J. Walsh, N. Viphakone, T.B. van Dijk, S. Philipsen, and S.A. Wilson. 2013. Chtop is a component of the dynamic TREX mRNA export complex. *EMBO J.* 32:473–486. http://dx.doi.org/10.1038/emboj.2012.342

Cléry, A., M. Blatter, and F.H. Allain. 2008. RNA recognition motifs: boring? Not quite. *Curr. Opin. Struct. Biol.* 18:290–298. http://dx.doi.org/10.1016/j.sbi.2008.04.002

Cox, J., and M. Mann. 2008. MaxQuant enables high peptide identification rates, individualized p.p.b.-range mass accuracies and proteome-wide protein quantification. *Nat. Biotechnol.* 26:1367–1372. http://dx.doi.org/10.1038/nbt.1511

Cox, J., and M. Mann. 2012. 1D and 2D annotation enrichment: A statistical method integrating quantitative proteomics with complementary high-throughput data. *BMC Bioinformatics*. 13:S12. http://dx.doi.org/10.1186/1471-2105-13-S16-S12

da Silva, M.R., G.A. Moreira, R.A. Gonçalves da Silva, É. de Almeida Alves Barbosa, R. Pais Siqueira, R.R. Teixera, M.R. Almeida, A. Silva Júnior, J.L. Fietto, and G.C. Bressan. 2015. Splicing regulators and their roles in cancer biology and therapy. *BioMed Res. Int.* 2015:150514. http://dx.doi.org/10.1155/2015/150514

Dobin, A., C.A. Davis, F. Schlesinger, J. Drenkow, C. Zaleski, S. Jha, P. Batut, M. Chaisson, and T.R. Gingeras. 2013. STAR: ultrafast universal RNA-seq aligner. *Bioinformatics.* 29:15–21. http://dx.doi.org/10.1093/bioinformatics/bts635

Hargous, Y., G.M. Hautbergue, A.M. Tintaru, L. Skrisovska, A.P. Golovanov, J. Stevenin, L.Y. Lian, S.A. Wilson, and F.H. Allain. 2006. Molecular basis of RNA recognition and TAP binding by the SR proteins SRp20 and 9G8. *EMBO J.* 25:5126–5137. http://dx.doi.org/10.1038/sj.emboj.7601385

Huang, Y., and J.A. Steitz. 2005. SRprises along a messenger's journey. *Mol. Cell.* 17:613–615. http://dx.doi.org/10.1016/j.molcel.2005.02.020

Hung, M.L., G.M. Hautbergue, A.P. Snijders, M.J. Dickman, and S.A. Wilson. 2010. Arginine methylation of REF/ALY promotes efficient handover of mRNA to TAP/NXF1. *Nucleic Acids Res.* 38:3351–3361. http://dx.doi.org/10.1093/nar/gkq033

Huppertz, I., J. Attig, A. D'Ambrogio, L.E. Easton, C.R. Sibley, Y. Sugimoto, M. Tajnik, J. König, and J. Ule. 2014. iCLIP: Protein–RNA interactions at nucleotide resolution. *Methods.* 65:274–287. http://dx.doi.org/10.1016/j.ymeth.2013.10.011

Kim, H.R., G.O. Lee, K.H. Choi, D.K. Kim, J.S. Ryu, K.E. Hwang, K.J. Na, C. Choi, J.H. Kuh, M.J. Chung, et al. 2016. SRSF5: a novel marker for small-cell lung cancer and pleural metastatic cancer. *Lung Cancer.* 99:57–65. http://dx.doi.org/10.1016/j.lungcan.2016.05.018

Kim, J., R.Y. Park, J.K. Chen, J. Kim, S. Jeong, and T. Ohn. 2014. Splicing factor SRSF3 represses the translation of programmed cell death 4 mRNA by associating with the 5′-UTR region. *Cell Death Differ.* 21:481–490. http://dx.doi.org/10.1038/cdd.2013.171

König, J., K. Zarnack, G. Rot, T. Curk, M. Kayikci, B. Zupan, D.J. Turner, N.M. Luscombe, and J. Ule. 2010. iCLIP reveals the function of hnRNP

particles in splicing at individual nucleotide resolution. *Nat. Struct. Mol. Biol.* 17:909–915. http://dx.doi.org/10.1038/nsmb.1838

Lai, M.C., R.I. Lin, and W.Y. Tarn. 2001. Transportin-SR2 mediates nuclear import of phosphorylated SR proteins. *Proc. Natl. Acad. Sci. USA.* 98:10154–10159. http://dx.doi.org/10.1073/pnas.181354098

Larsen, M.R., T.E. Thingholm, O.N. Jensen, P. Roepstorff, and T.J. Jørgensen. 2005. Highly selective enrichment of phosphorylated peptides from peptide mixtures using titanium dioxide microcolumns. *Mol. Cell. Proteomics.* 4:873–886. http://dx.doi.org/10.1074/mcp.T500007-MCP200

Larsen, S.C., K.B. Sylvestersen, A. Mund, D. Lyon, M. Mullari, M.V. Madsen, J.A. Daniel, L.J. Jensen, and M.L. Nielsen. 2016. Proteome-wide analysis of arginine monomethylation reveals widespread occurrence in human cells. *Sci. Signal.* 9:rs9. http://dx.doi.org/10.1126/scisignal.aaf7329

Lin, S., R. Xiao, P. Sun, X. Xu, and X.D. Fu. 2005. Dephosphorylation-dependent sorting of SR splicing factors during mRNP maturation. *Mol. Cell.* 20:413–425. http://dx.doi.org/10.1016/j.molcel.2005.09.015

Lou, H., K.M. Neugebauer, R.F. Gagel, and S.M. Berget. 1998. Regulation of alternative polyadenylation by U1 snRNPs and SRp20. *Mol. Cell. Biol.* 18:4977–4985. http://dx.doi.org/10.1128/MCB.18.9.4977

Love, M.I., W. Huber, and S. Anders. 2014. Moderated estimation of fold change and dispersion for RNA-seq data with DESeq2. *Genome Biol.* 15:550. http://dx.doi.org/10.1186/s13059-014-0550-8

Maslon, M.M., S.R. Heras, N. Bellora, E. Eyras, and J.F. Cáceres. 2014. The translational landscape of the splicing factor SRSF1 and its role in mitosis. *eLife.* 6:e02028. http://dx.doi.org/10.7554/eLife.02028

Masuyama, K., I. Taniguchi, N. Kataoka, and M. Ohno. 2004. SR proteins preferentially associate with mRNAs in the nucleus and facilitate their export to the cytoplasm. *Genes Cells.* 9:959–965. http://dx.doi.org/10.1111/j.1365-2443.2004.00774.x

Michlewski, G., J.R. Sanford, and J.F. Cáceres. 2008. The splicing factor SF2/ASF regulates translation initiation by enhancing phosphorylation of 4E-BP1. *Mol. Cell.* 30:179–189. http://dx.doi.org/10.1016/j.molcel.2008.03.013

Müller-McNicoll, M., V. Botti, A.M. de Jesus Domingues, H. Brandl, O.D. Schwich, M.C. Steiner, T. Curk, I. Poser, K. Zarnack, and K.M. Neugebauer. 2016. SR proteins are NXF1 adaptors that link alternative RNA processing to mRNA export. *Genes Dev.* 30:553–566. http://dx.doi.org/10.1101/gad.276477.115

Nakayama, Y., A. Wada, R. Inoue, K. Terasawa, I. Kimura, N. Nakamura, and A. Kurosaka. 2014. A rapid and efficient method for neuronal induction of the P19 embryonic carcinoma cell line. *J. Neurosci. Methods.* 227:100–106. http://dx.doi.org/10.1016/j.jneumeth.2014.02.011

Poser, I., M. Sarov, J.R. Hutchins, J.K. Hériché, Y. Toyoda, A. Pozniakovsky, D. Weigl, A. Nitzsche, B. Hegemann, A.W. Bird, et al. 2008. BAC TransgeneOmics: a high-throughput method for exploration of protein function in mammals. *Nat. Methods.* 5:409–415. http://dx.doi.org/10.1038/nmeth.1199

Rappsilber, J., M. Mann, and Y. Ishihama. 2007. Protocol for micro-purification, enrichment, pre-fractionation and storage of peptides for proteomics using StageTips. *Nat. Protoc.* 2:1896–1906. http://dx.doi.org/10.1038/nprot.2007.261

Richter, F.M., H.H. Hsiao, U. Plessmann, and H. Urlaub. 2009. Enrichment of protein-RNA crosslinks from crude UV-irradiated mixtures for MS analysis by on-line chromatography using titanium dioxide columns. *Biopolymers.* 91:297–309. http://dx.doi.org/10.1002/bip.21139

Rigbolt, K.T., T.A. Prokhorova, V. Akimov, J. Henningsen, P.T. Johansen, I. Kratchmarova, M. Kassem, M. Mann, J.V. Olsen, and B. Blagoev. 2011. System-wide temporal characterization of the proteome and phosphoproteome of human embryonic stem cell differentiation. *Sci. Signal.* 4:rs3. http://dx.doi.org/10.1126/scisignal.2001570

Sanford, J.R., N.K. Gray, K. Beckmann, and J.F. Cáceres. 2004. A novel role for shuttling SR proteins in mRNA translation. *Genes Dev.* 18:755–768. http://dx.doi.org/10.1101/gad.286404

Sapra, A.K., M.L. Ankö, I. Grishina, M. Lorenz, M. Pabis, I. Poser, J. Rollins, E.M. Weiland, and K.M. Neugebauer. 2009. SR protein family members display diverse activities in the formation of nascent and mature mRNPs in vivo. *Mol. Cell.* 34:179–190. http://dx.doi.org/10.1016/j.molcel.2009.02.031

Shimoni-Sebag, A., I. Lebenthal-Loinger, L. Zender, and R. Karni. 2013. RRM1 domain of the splicing oncoprotein SRSF1 is required for MEK1-MAPK-ERK activation and cellular transformation. *Carcinogenesis.* 34:2498–2504. http://dx.doi.org/10.1093/carcin/bgt247

Sinha, R., E. Allemand, Z. Zhang, R. Karni, M.P. Myers, and A.R. Krainer. 2010. Arginine methylation controls the subcellular localization and functions of the oncoprotein splicing factor SF2/ASF. *Mol. Cell. Biol.* 30:2762–2774. http://dx.doi.org/10.1128/MCB.01270-09

Snijders, A.P., G.M. Hautbergue, A. Bloom, J.C. Williamson, T.C. Minshull, H.L. Phillips, S.R. Mihaylov, D.T. Gjerde, D.P. Hornby, S.A. Wilson, et al. 2015. Arginine methylation and citrullination of splicing factor proline- and glutamine-rich (SFPQ/PSF) regulates its association with mRNA. *RNA.* 21:347–359. http://dx.doi.org/10.1261/rna.045138.114

Surendranath, V., M. Theis, B.H. Habermann, and F. Buchholz. 2013. Designing efficient and specific endoribonuclease-prepared siRNAs. *Methods Mol. Biol.* 942:193–204. http://dx.doi.org/10.1007/978-1-62703-119-6_11

Swanson, C.M., N.M. Sherer, and M.H. Malim. 2010. SRp40 and SRp55 promote the translation of unspliced human immunodeficiency virus type 1 RNA. *J. Virol.* 84:6748–6759. http://dx.doi.org/10.1128/JVI.02526-09

Swartz, J.E., Y.C. Bor, Y. Misawa, D. Rekosh, and M.L. Hammarskjold. 2007. The shuttling SR protein 9G8 plays a role in translation of unspliced mRNA containing a constitutive transport element. *J. Biol. Chem.* 282:19844–19853. http://dx.doi.org/10.1074/jbc.M701660200

Tintaru, A.M., G.M. Hautbergue, A.M. Hounslow, M.L. Hung, L.Y. Lian, C.J. Craven, and S.A. Wilson. 2007. Structural and functional analysis of RNA and TAP binding to SF2/ASF. *EMBO Rep.* 8:756–762. http://dx.doi.org/10.1038/sj.embor.7401031

van der Houven van Oordt, W., M.T. Diaz-Meco, J. Lozano, A.R. Krainer, J. Moscat, and J.F. Cáceres. 2000. The $MKK_{3/6}$-p38–signaling cascade alters the subcellular distribution of hnRNP A1 and modulates alternative splicing regulation. *J. Cell Biol.* 149:307–316. http://dx.doi.org/10.1083/jcb.149.2.307

Wang, H., X. Bian, L. Xia, X. Ding, R. Müller, Y. Zhang, J. Fu, and A.F. Stewart. 2014. Improved seamless mutagenesis by recombineering using *ccdB* for counterselection. *Nucleic Acids Res.* 42:e37. http://dx.doi.org/10.1093/nar/gkt1339

Wang, Z., M. Kayikci, M. Briese, K. Zarnack, N.M. Luscombe, G. Rot, B. Zupan, T. Curk, and J. Ule. 2010. iCLIP predicts the dual splicing effects of TIA-RNA interactions. *PLoS Biol.* 8:e1000530. http://dx.doi.org/10.1371/journal.pbio.1000530

Wright, L.P., and M.R. Philips. 2006. Thematic review series: Lipid posttranslational modifications. CAAX modification and membrane targeting of Ras. *J. Lipid Res.* 47:883–891. http://dx.doi.org/10.1194/jlr.R600004-JLR200

Yeo, G.W., N.G. Coufal, T.Y. Liang, G.E. Peng, X.D. Fu, and F.H. Gage. 2009. An RNA code for the FOX2 splicing regulator revealed by mapping RNA-protein interactions in stem cells. *Nat. Struct. Mol. Biol.* 16:130–137. http://dx.doi.org/10.1038/nsmb.1545

Zahler, A.M., K.M. Neugebauer, W.S. Lane, and M.B. Roth. 1993. Distinct functions of SR proteins in alternative pre-mRNA splicing. *Science.* 260:219–222. http://dx.doi.org/10.1126/science.8385799

Zhou, Z., and X.D. Fu. 2013. Regulation of splicing by SR proteins and SR protein-specific kinases. *Chromosoma.* 122:191–207. http://dx.doi.org/10.1007/s00412-013-0407-z